ELBOW JOINT CONTACT MECHANICS: MULTIBODY AND FINITE ELEMENT METHODS

A THESIS IN
Mechanical Engineering

Presented to the Faculty of the University
of Missouri – Kansas City in partial fulfillment of
the requirements for the degree

MASTER OF SCIENCE

by
MOHSEN SHARIFI RENANI

B.S. Isfahan University of Technology, 2014

Kansas City, Missouri
2017

ELBOW JOINT CONTACT MECHANICS: MULTIBODY AND FINITE ELEMENT METHODS

Mohsen Sharifi Renani, Candidate for the Master of Science Degree

University of Missouri – Kansas City, 2017

ABSTRACT

Only a few millimeter thick articular cartilage is a very specialized connective tissue which withstands high compressive and shear forces while protecting the bone from excessive loading, and provides a smooth articulation for the joint. Better understanding of elbow cartilage contact mechanics can provide a valuable insight into cartilage degeneration mechanisms and osteoarthritis development. Computational modeling is a very efficient tool that helps us gain better understanding of joint biomechanics, particularly elbow joint contact mechanics. This tool can predict parameters that are not feasible to measure experimentally, decrease the cost of physical experiment, help develop better rehabilitation and surgical protocols, and finally improve patient care. The objectives of the study presented here were first, to develop subject specific finite element (FE) models of the isolated ulno-humeral joint of the elbow and validate these models against experiment measurements. Second, to develop multibody (MB) models of the same joints with the humerus cartilage represented with discrete rigid bodies interacting with the ulna cartilage with deformable contacts. Third, to optimize the deformable contact parameters used in the MB models to validated FE models and assess the effect of grid sizes on the contact predictions. These models allow for the prediction of cartilage contact characteristics including maximum and average contact pressure (MPa), and contact

area (mm2) under different loading conditions and during activities in the anatomic elbow joint. Finally, the results from optimization indicated that the selection of contact parameters is very critical for accurate prediction of contact mechanics within the MB models of ulno-humeral joints.

The faculty listed below, appointed by the Dean of the School of Graduate Studies, have examined the dissertation titled "Elbow Joint Contact Mechanics: Multibody and Finite Element Methods" presented by Mohsen Sharifi Renani, candidate for the Master of Science in Mechanical Engineering degree, and certify that in their opinion it is worthy of acceptance.

Supervisory Committee

Antonis P. Stylianou, Ph.D., Committee Chair
Department of Civil & Mechanical Engineering

Ganesh Thiagarajan, Ph.D.
Department of Civil & Mechanical Engineering

Gregory W. King, Ph.D.
Department of Civil & Mechanical Engineering

TABLE OF CONTENTS

ILLUSTRATIONS

TABLES

Table Page

ACKNOWLEDGMENTS

The project was partially funded by the School of Graduate Studies research grant program, University of Missouri- Kansas City (UMKC).

First and foremost I would like to acknowledge my supervisor, Dr. Antonis P. Stylianou who has provided me a great opportunity to work in the Musculoskeletal Biomechanics Research Laboratory and enormously supported me for accomplishment of my research goal. I would also like to acknowledge Dr. Akin Cil for his guidance and support during this process. Finally, I would like to thank my lab partners, Munsur Rahman and Jonathan Parman for helping me troubleshoot problems.

CHAPTER 1

INTRODUCTION

The elbow is one of the most rewarding joint which allows for the flexion and extension of the forearm relative to the upper arm, as well as rotation of the forearm and wrist. The elbow joint consists of three bone articulations: the ulno-humeral, radiocapitellar, and proximal radioulnar joints located within a synovial-lined joint capsule (Fig 1.1). The ulno-humeral joint is a hinge joint which is formed by the articulation of the central waist of the humeral trochlea and the ulnar trochlear notch. The radiocapitellar joint consists the articulation of the concave cartilage of radial head and the convex cartilage of capitellum. The proximal radioulnar joint is formed by the circumference of the radial head cartilage and the radial notch, a small gap on the lateral side of the coronoid process of the ulna (Martin & Sanchez, 2013).

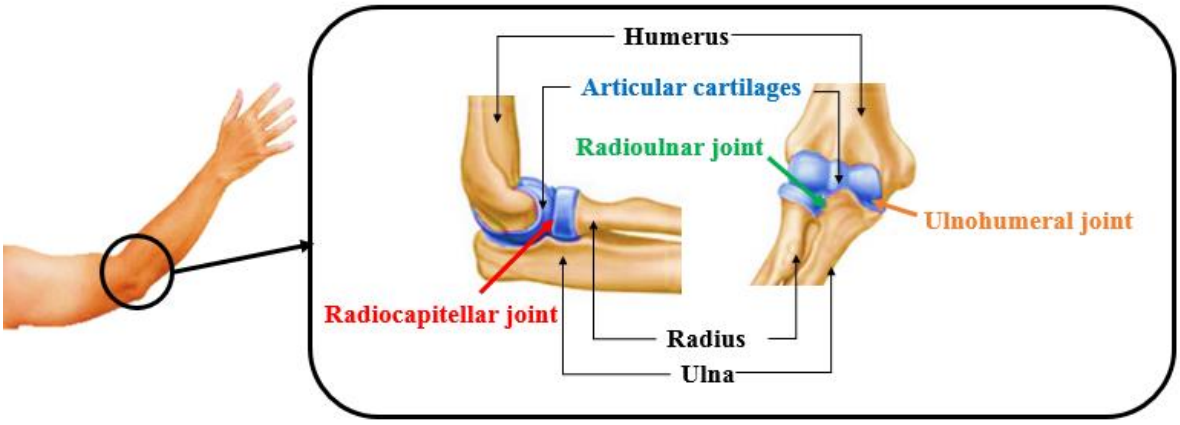

Figure 1.1. Elbow Joint-bones.

The joint capsule is a strong and fibrous soft tissue, thickened medially and laterally to form collateral ligaments, which stabilize the flexing and extending motion of the arm (Fig 1. 2). The posterior capsule extends proximally above the olecranon fossa, distally along the

medial and lateral articular margins of the greater sigmoid notch, and laterally becomes continuous with the annular ligament. The anterior capsule attaches proximally above the coronoid and radial fossae, distally to the edge of the coronoid process, and laterally to the annular ligament (Bryce & Armstrong, 2008).

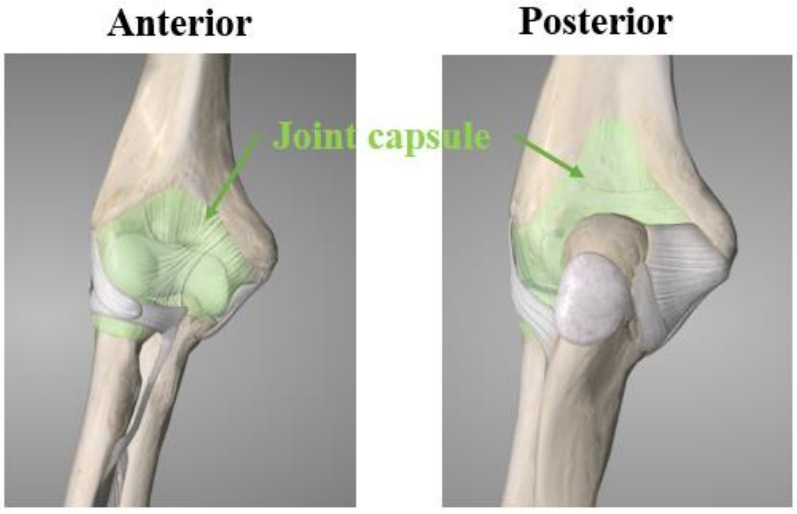

Figure 1.2. Elbow joint capsule.

The elbow joint is constrained by two major ligament complexes, the medial collateral ligament (MCL) and the lateral collateral ligament (LCL) complex. The MCL complex itself has three parts including anterior, posterior, and transverse bundles (Fig 1.3a). The anterior bundle attaches to the medial epicondyle of the humerus superiorly and the sublime tubercle on the coronoid process of the ulna inferiorly. The posterior bundle of the MCL runs from the medial epicondyle to the medial olecranon. The transverse bundle lies only on the ulna bone and runs from medial olecranon to medial coronoid process (B.F. Morrey, 2000). Unlike the anterior and posterior bundles which provide a significant stability against valgus force, the

transverse bundle has no function in joint stability (Bryce & Armstrong, 2008; B.F. Morrey, 2000; B. F. Morrey & An, 1985).

The lateral collateral ligament (LCL) is a Y-shaped ligamentous complex composed four segments, including radial collateral ligament (RCL), the latera ulnar collateral ligament (LUCL), the annular ligament (AL), and the accessory lateral collateral ligament (ALCL) (Fig 1.3b). The radial collateral ligament (RCL) originates from lateral epicondyle of humerus, and attached inferiorly to the annular ligament deep to the common extensor tendon. LUCL also originates from lateral humerus epicondyle, however, its distal attachment is on the crista supinatorum tubercle of the ulna and partially on annular ligament. It provides varus and posterolateral stability. The AL is a strong band of tissue that maintains the radial head in contact with ulna and runs from the anterior to the posterior rim of the lesser sigmoid notch. The ALCL is a further stabilizer of the annular ligament during varus stress and it originates from crista supinatorum tubercle of the ulna and inserters to distal lateral rim of the annular ligament (Bryce & Armstrong, 2008; M. Rahman, Cil, A., Johnson, M., Lu, Y., Guess, T.M., 2014).

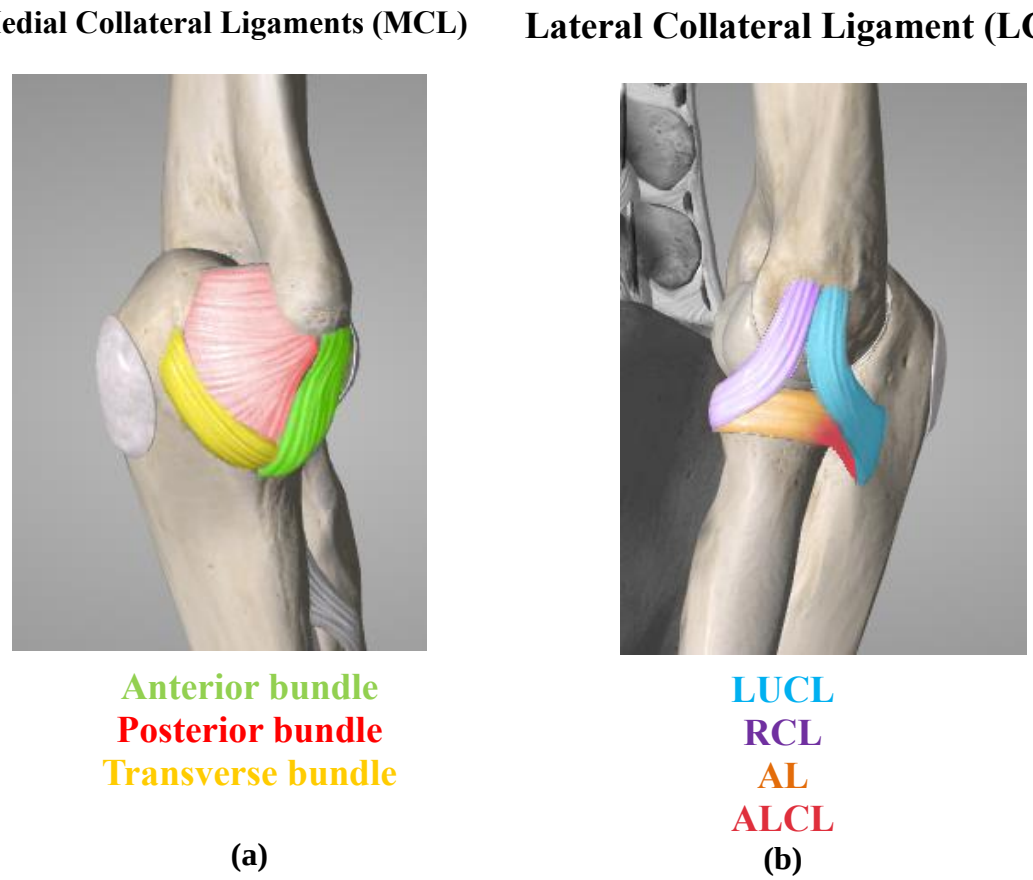

Figure 1.3. Ligaments around the elbow joint (a) medial and (b) lateral collateral ligament complex.

The muscles around the elbow joint can be categorized into three groups based on their biomechanical functions. These muscle groups are flexor, extensor, and forearm rotators. The flexor group is composed of the brachailis, biceps brachii, and the brachioradialis muscles and they flex the arm by decreasing the angle between the forearm and upper arm (Fig 1.4). The brachailis lies deeper than the biceps, originates from the anterior surface of the distal half of the humerus and inserts into the rough depression on the anterior surface of the coronoid process of the ulna. The biceps brachii, commonly known as the biceps, a two-heads muscle lies one the upper arm between the shoulder and the elbow. The long and short heads of bicep

connected to the superaglenoid tubercle and coracoid process of the scapula respectively and then both join together and insert into proximal radius. In addition to flexion of the forearm, it also supinates the elbow. The brachioradialis muscle is a multifunction muscle, it is involved in flexion, supination, and pronation. Its origin and insertion are located on the distal upper two-thirds of the lateral supracondylar ridge of the humerus bone and styloid process of the radius bone respectively.

The extensor group includes the triceps brachii and anconeus muscles which straighten the arm by increasing the angle of humerus and ulna, until the olecranon locks into the olecranon fossa of the humerus. The triceps is placed on the posterior side of humerus and its origin and insertion are placed on the scapula and the olecranon of the ulna. The anconeus is a relatively smaller muscle which runs from the distal end of the humerus to the olecranon.

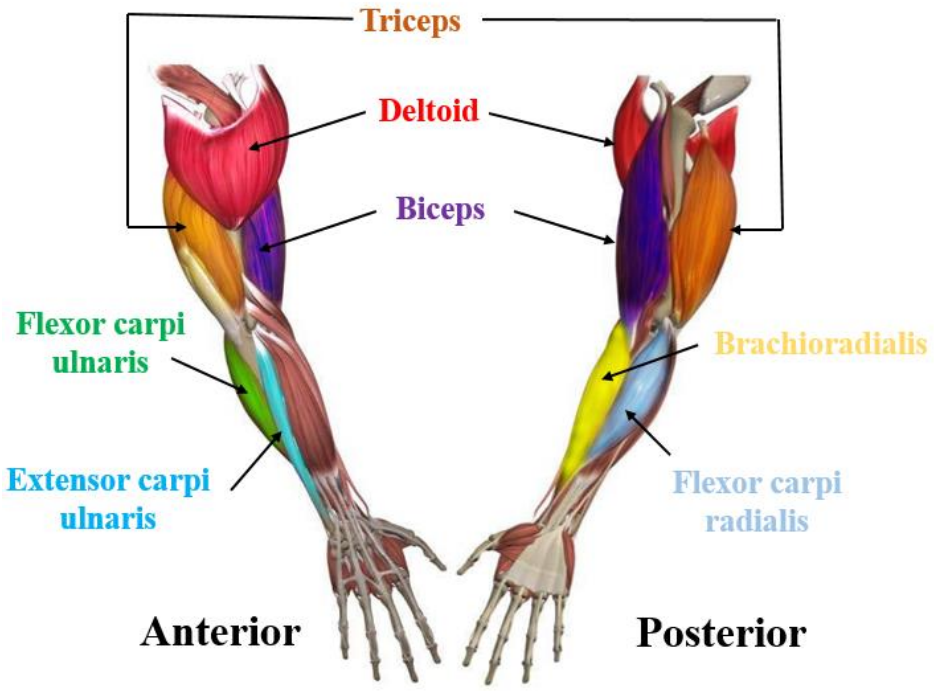

Figure 1.4. Upper arm muscles.

The pronator teres and the supinator are the two muscles that cross the elbow joint and provide rotational movement of the forearm. The pronator teres begins from the medial epicondyle of the humerus and medial side of coronoid process of ulna, and ends to middle of lateral surfaces of radius. The supinator muscle is a broad, cylindrical-shaped muscle in the forearm that normally curves around the upper third of the radius and connects the lateral epicondyle of the humerus to the radius.

The ends of the elbow bones are covered with articular cartilage, hyaline cartilage with 2 to 4 mm thickness that allow the bones to glide over each other with very little friction (Fig 1.5). Generally, articular cartilage is made of two phases, a fluid and a solid phase. The solid phase, a dense extracellular matrix (ECM) composed of a water, collagen, chondrocyte, and proteoglycans, other noncollagenous proteins, and glycoproteins. All these components together contribute in retaining the water within the ECM and providing the unique mechanical properties for the cartilage. The water alone represents the 80% of the wet weight of the cartilage tissue.

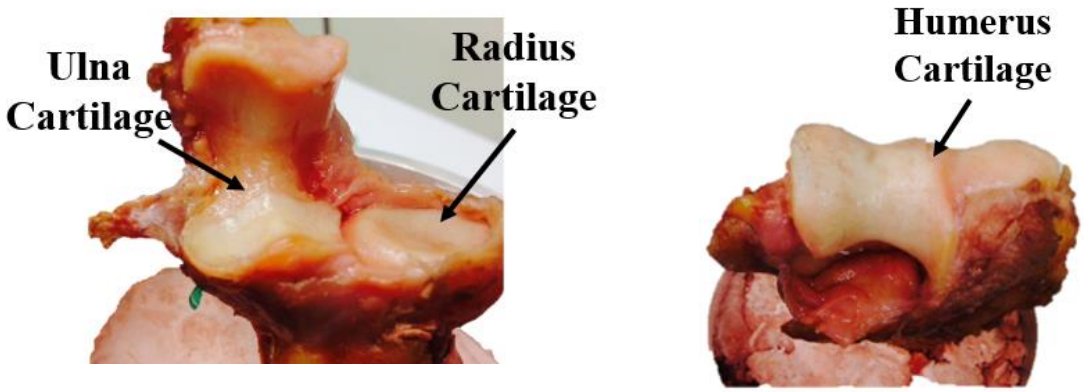

Figure 1.5. Articular cartilages of elbow joint, (a) ulna and radius and (b) humerus.

According to the collagen fibrils positioning and chondrocytes density, articular cartilage is divided into three main zones, superficial, middle, and deep zone (Fig 1.6). The superficial zone captures almost 10% to 20% of the cartilage volume and it protects the deeper layer from shear stress. The collagen fibers are organized parallel to the articular surface. The middle zone makes up the 40% to 60% of the cartilage volume and functions as a first resistance of the compressive force. This zone contains chondrocytes with a low density and thicker collagen fibrils which are structured obliquely. The deep zone represents 30% of the cartilage volume and plays the greatest role in resisting the compressive force. Its collagens has the largest diameters and are organized perpendicularly to the cartilage surface (Sophia Fox, Bedi et al. 2009).

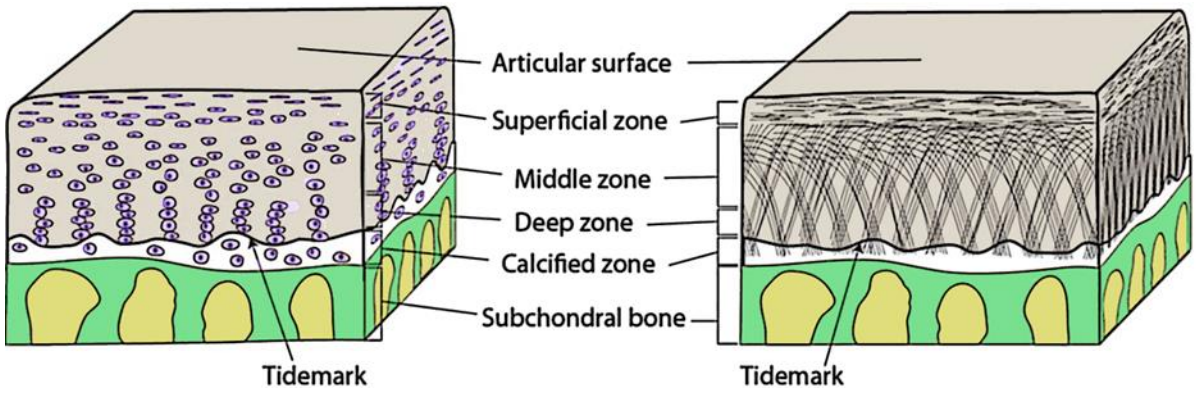

Figure 1.6. Cartilage structure (Zhang, Blalock, & Wang, 2015).

Because of the load bearing role of articular cartilage, its injury is very common which leads to musculoskeletal disorders and morbidity. Most important, since articular cartilage lacks blood vessels, nerves, and lymph node, it has limited capacity for tissue repair and healing. Therefore, preventing and treating articular cartilage has been recognized as one the most challenging issues for the patient, surgeons, and researchers. Articular cartilage can be damaged by injury or normal wear and tear. Degenerative joint disease or degenerative

arthritis, osteoarthritis (OA) is the most common chronic condition of the joints, affecting approximately 27 million Americans. It leads to joint swelling, pain, stiffness and decreased ranged of motion of the elbow joint. Increased knowledge in joint contact mechanics, particularly ulno-humerus joint could provide a greater insight on the joint environment, functionality, degenerative diseases, and consequently, it can lead to development of better preventative approaches to joint disease, assist in improvement of prosthesis designs, surgical treatment, and rehabilitation. Since direct measurement of the in-vivo joint loads is not feasible, computational models have to be implemented for predictions. Finite element and multibody analysis are two of the most popular modeling techniques for joint contact mechanics. Finite element methods are generally used for specific tissues in static and quasi-static models. On the other side, multibody computational models are ideal for use in dynamic concurrent simulations and are computationally efficient. However, accurate prediction of cartilage contact pressures in the multibody framework is challenging.

The broad objective of this study was to provide a work flow for developing and validating ulno-humeral computational models simulating joint contact mechanics. The first specific objective of this project was to measure the contact pressure and contact area within the elbow joint during a compression test using a tactile sensor. The second objective was to develop finite element and multibody models of the specimens and validate them against the experimental measurements. The last and most important one was to determine the optimized element size and contact parameters of articular cartilage used in multibody model based on developed finite element model. Hence, optimized contact parameters can be implemented into previously developed multibody models leading to correct prediction of the contact force and contact area and also realistic simulation of clinical scenarios. Moreover, validated finite

element models can be used for simulating the behavior of articular cartilage in response to the different elbow joint prostheses.

The second chapter describes the contact pressure measurements within the elbow joint during a compression test using a tactile sensor. It also explains the methodology for developing finite element model of elbow joints from medical images for studying joint contact mechanics. In the third chapter, developing of multibody elbow joint models with discretized humerus cartilage is presented step by step. The FE based optimization approach was performed to find the optimum discrete size and contact parameters used in each models. Then, the response of optimized models was evaluated under different loading situations and against the validated FE models in subject specific cases. The conclusion of the manuscript is provided in the last chapter.

CHAPTER 2

ULNA-HUMERUS CONTACT MECHANICS: FINITE ELEMENT ANALYSIS AND EXPERIMENTAL MEASUREMENTS USING A TACTILE PRESSURE SENSOR

2.1 Introduction

Articular cartilage endures high compressive and shearing forces while protecting the bone from excessive contact pressure. Articular cartilage within the elbow joint withstands repetitive mechanical forces that are about 50% body weight during activities of daily living (Safran, Ahmad, & Elattrache, 2005). Abnormal stress acting on cartilage is believed to be one of the leading causes for cartilage degeneration and osteoarthritis development (Dekel & Weissman, 1978). A better understanding of elbow cartilage contact mechanics can provide insight into our understanding of cartilage degeneration mechanisms and assist in the development of elbow rehabilitation protocols. Computational models, such as multibody analysis and finite element models are immensely valuable tools to study elbow joint contact mechanics. These models can enhance our understanding of tissue function, tissue interactions, and loading conditions during dynamic activities. Moreover, models can be used to predict quantities that are very hard or often time impossible to measure experimentally, and improve patient specific treatment.

Multiple studies have investigated biomechanics of the knee and hip joints using finite element (FE) models (A. E. Anderson, Ellis, Maas, Peters, & Weiss, 2008; Erdemir, 2016; Harris et al., 2012; Kiapour et al., 2014; Li et al., 2014; Meng, Jin, Wilcox, & Fisher, 2014; Mootanah et al., 2014). However, computational models have been greatly underutilized in studies of the elbow joint. Wake et al. (2004) (Wake, Hashizume, Nishida, Inoue, &

Nagayama, 2004), investigated the effects of compressive forces on the fracture-dislocations the elbow joint at different flexion angles. The stress concentration across the elbow joint was analyzed through simple two dimensional finite element models along with the corresponding experiments. They showed that the stress concentration areas, representing the location of the fracture, moved from the coronoid process to the olecranon as the position changed from extension to flexion. Willing et al. (2013) (R. T. Willing, Lalone, Shannon, Johnson, & King, 2013) studied elbow joint contact mechanics experimentally and numerically. A three dimensional subject specific finite element model of the elbow joint was created and the contact area was computed numerically under a compressive load of 80N holding the joint at 20° of flexion. The contact area from a single cadaveric elbow joint under the same static, axially loaded condition was measured using a casting method. The FE predicted contact areas were in good agreement with the contact areas identified experimentally. However, since identifying the cartilage contact pressure distribution is not possible through the casting method, the FE model predicted contact pressure distribution over the articular cartilage was not evaluated. Knowledge of contact pressure distribution is critical for better understanding the load-bearing function of cartilage, pathogenesis of joint diseases such as osteoarthritis, and design of elbow joint arthroplasties (Ateshian, Henak, & Weiss, 2015). Recently, Kim and Miller (2016) (Kim & Carl Miller, 2016) used Fuji pressure sensitive film to validate FE predicted contact pressure and contact area on the radial head of a cadaveric elbow joint. The cartilage thickness used in the FE analysis was assumed to be uniform while in reality the thickness of the cartilage varies in different regions (Schenck, Athanasiou, Constantinides, & Gomez, 1994). Moreover, the contact pressure on the ulno-humeral joint was not computed. While previous studies provided some valuable insight about the elbow cartilage contact

mechanics using FE models, a complete description of articular cartilage contact pressure distribution of the ulno-humeral joint is still unavailable.

Therefore, the overall objectives of this project was to study the contact mechanics of the ulno-humeral joint through: (1) developing subject specific finite element models of the ulno-humeral joint, (2) direct comparison of FE-computed contact pressure distribution against experimental measurements taken with a tactile sensor, and (3) investigating the model's sensitivity to the cartilage mechanical properties.

2.2 Methods

Cadaveric Preparation and Imaging

Two fresh-frozen cadaveric elbow specimens (right and left arm) from a 69 years old male were used in this study. All soft tissue around the joint was removed while the joint capsule and ligaments were kept intact. The specimens were truncated to 15cm above and below the elbow joint. To facilitate the alignment of the elbow geometries in the computational models, three custom made ABS plastic localizers that contained two perpendicular tubes filled with mustard (visible in MRI) were attached to each bone using titanium screws (Fig. 2.1a). Magnetic resonance imaging (MRI) of the elbows was done by a clinical Siemens 1.5 T machine (Siemens, Siemens Medical Solutions, PA) with acquisition parameters: MRI type: 3D, image resolution 256 x 232, slice thickness 0.5mm, and spacing between slices 0.1mm.

Physical Experiment

The contact pressure across the articular cartilages within the elbow joint was measured using a tactile sensor (Model-4201, Tekscan Inc., Boston, MA, USA) under three different loading conditions. The sensor was calibrated using 3 point calibration (approximately 25%,

75%, and 125% of the maximum axial expected load) by compressing the sensor between two silicon-rubber sheets of 2 mm thickness (Wilharm, Hurschler, Dermitas, & Bohnsack, 2013). After calibration, the sensor was sealed between two layers of Tegaderm adhesive waterproof transparent dressing (3M, NexcareTM) (Wang et al., 2014; Wang, Chen, Torzilli, Warren, & Maher, 2014). An incision was made on the anterior joint capsule to allow insertion of the sensor. A smaller incision was made on the posterior joint capsule so that sutures attached to the sensor could be used to guide the sensor to the correct position within the joint. The sensor was inserted from the anterior side and pulled out from posterior. Finally, the sensor was sutured to the joint capsule anteriorly and posteriorly to stabilize the sensor inside the joint (Fig. 2.1b).

The specimens were placed at 20° flexion in a bi-axial Instron 8821 (Instron, Norwood, MA, USA) mechanical testing machine with attached load cell of 300N. A custom made aluminum 20 degree jig was attached to the fixtures for adjusting the flexion angle at 20°. The humerus, ulna, and radius were cemented 5 cm deep into custom made aluminum cups. First, the humerus bone was cemented into the top cup at 0 degrees and attached to the top ram of the Instron machine. Then, the radius and ulna were kept in the neutral position and cemented into to bottom cup at 20° degree flexion.

A point cloud was collected at the initial position using an Optotrak rigid probe (NDI, Waterloo, Ontario, Canada). This data was used to transfer the geometries from the MRI coordinate system to the experimental coordinate system and to align the geometries later in the computational model. Three different axial loads: 80N, 110N, and 140N with a rate of 1mm/min were applied to the proximal humerus and maintained for 10 min to allow viscoelastic deformation of cartilage to become constant [3]. Contact pressure data was

collected during the entire experiment, but only the last frame of 10 minutes was used for evaluation of the finite element model (Fig. 2.1c).

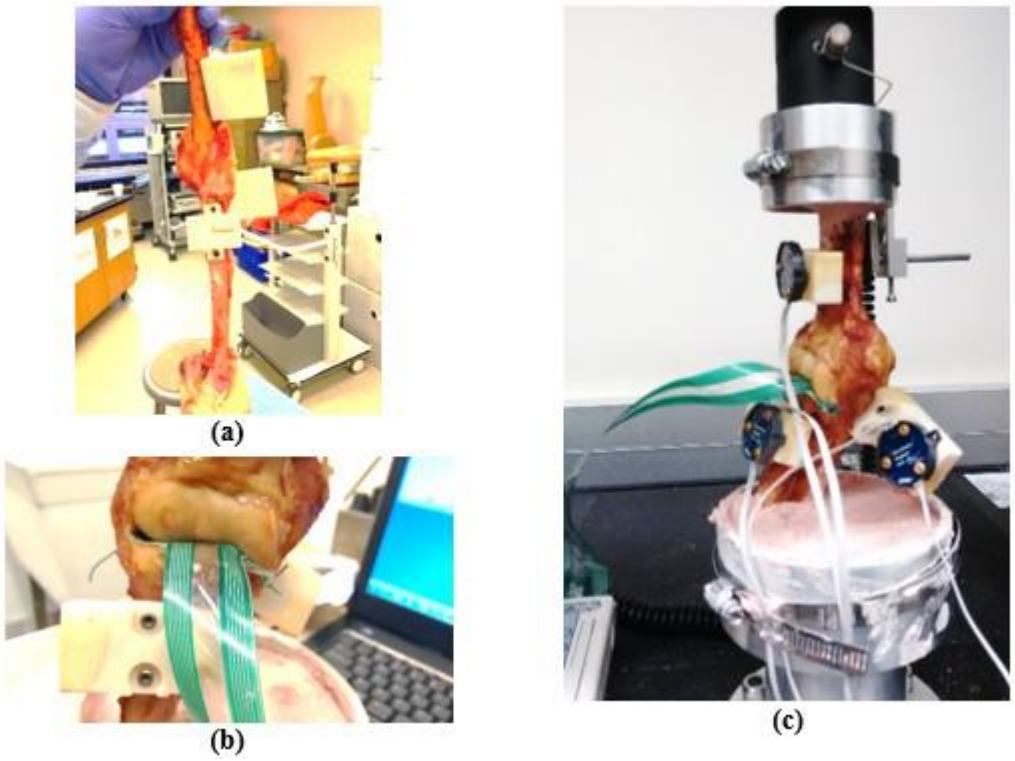

Figure 2.1. Cadaver after removing soft tissue and with attached localizers (a), position of the sensor inside the joint (b), and complete cadaver testing set up (c).

Finite Element Modeling

Three-dimensional geometries of the humerus, radius, and ulna, as well as their localizers were created from Magnetic Resonance Imaging (MRI). Auto thresholding, manual segmentation and subtraction of cartilage geometries from bones were employed in MIMICS (Mimics software, Materialise, Leuven, Belgium) to get the 3D surface geometries. The created 3D geometries were then imported into Meshlab (Visual Computing Lab - ISTI – CNR http://meshlab.sourceforge.net/) for post-processing that included smoothing, removing spikes, and noise reduction.

A least-squares best fit algorithm was implemented to align the geometries with the point cloud collected from the initial position of the experiment. The alignment was conducted in ADAMS software (MSC Software Corporation, Santa Ana, CA) by applying a linear stiffness matrix between the localizer points and their corresponding experimental cloud points (Fig. 2.2a). After alignment, the 3D solid model of the elbow joint including the osseous and cartilage geometries was converted into solid 4-node tetrahedral elements. The element size for cartilages and bones were assumed to be approximately 1mm and 2mm respectively (Fig. 2.2b). The meshed geometries were then imported into PreView (version 1.7; mrl.sci.utah.edu/software.php) for preprocessing. Since experimental contact measures were only possible from the ulno-humeral articulation, the radius bone and cartilage were not included in the model.

Bones were modeled as rigid bodies and cartilages were modeled with Moony-Rivlin hyper elastic material (E=0.7 MPa, v=0.47) (Schenck, et al., 1994; R. T. Willing, et al., 2013). Cartilage to bone and cartilage to cartilages contact surfaces were defined as rigid tie and frictionless surface to surface contacts respectively (Erdemir, 2016). To replicate the experimental conditions, the ulna was constrained in all degrees of freedom and the humerus was allowed to translate along the distal–proximal axis. Three different loads were applied on the center of the humerus and the simulation was run in FEBio (version 2.4; mrl.sci.utah.edu/software.php) for 7 seconds to allow the contact pressure across the articular cartilage to reach a stable value. For each case, the load was ramped over 0.6 s to the corresponding maximum load and then kept constant for the rest of the simulation. The contact pressure distribution (third principal stress) across the articular cartilage, its maximum value,

and the contact area were computed at the end of the simulation and compared with the experimentally collected data.

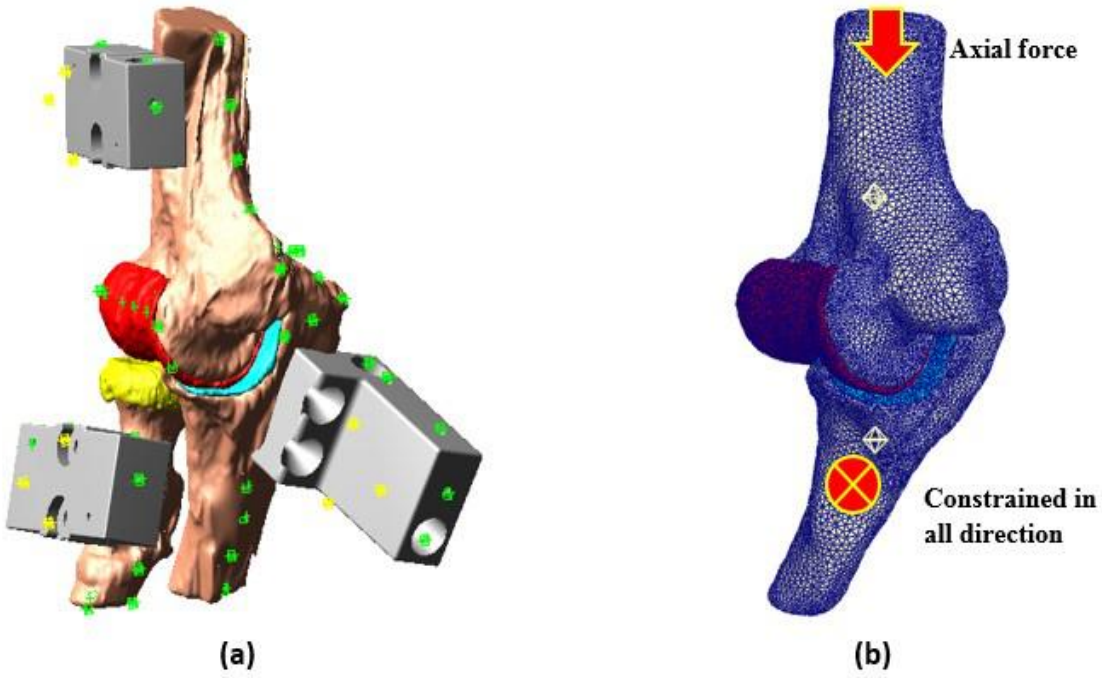

Figure 2.2. Aligned model in ADAMS (a) and Finite Element model (b).

The FE model convergence was evaluated by comparing the model predicted maximum contact pressure for cartilage element size of 1mm, 0.7mm, and 0.5mm under 110N compression load. The results show that the differences between all cases were less than 0.05. Therefore, models of 1mm element size were used for all simulations and analysis.

Parametric Analysis

One-at-a-time parametric analysis were performed to investigate the sensitivity of the model's contact predictions to cartilage material properties, such as Young's modulus (E) and Poisson's ratio (v). First, the baseline cartilage Young's modulus was altered by ±20% while the Poisson's ratio was kept constant. Then, Young's modulus was kept constant and

the Poisson's ratio was varied from 0.43 (bulk to shear modulus of 10:1) as the minimum value to 0.49 (bulk to shear modulus of 100:1) as the maximum value with increments of 0.01. The contact area, average, and peak contact pressures were computed for each case (A. E. Anderson, et al., 2008; Hamby, 1995; Kiapour, et al., 2014).

2.3 Results

The FE predicted and the experimentally measured contact pressure distribution over the humerus cartilage for the three loading scenarios are shown in Figure 2.3. Overall, the FE-computed contact pressure distributions are in a very good agreement with the experimental measurements.

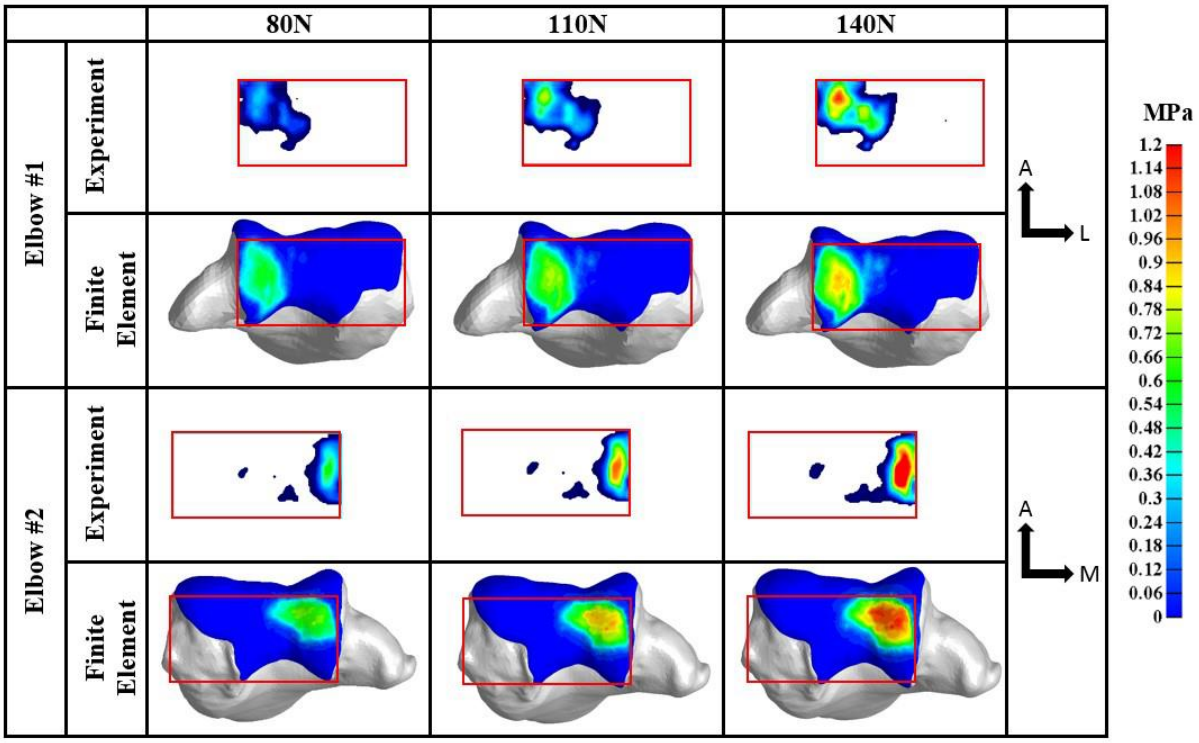

Figure 2.3. The experimentally measured and FE-computed contact pressure distribution within the ulno-humeral joint across 3 different loading conditions. A, L, and M markers the anterior, lateral, and medial direction of the elbow joint.

Peak and mean contact pressure

Quantitatively, the FE predicted and measured peak and mean contact pressures and the contact areas are presented in Figure 4. The peak contact pressure predicted by the FE models increased from 0.75±0.1 MPa to 1.15±0.18 MPa and where the mean contact pressure increased from 0.36±0.018 MPa to 0.48±0.02 MPa as the applied load was increased from 80 to 140N. Experimental measurements demonstrated a similar trend with the peak and mean contact pressures increasing from 0.64±0.1 MPa and 0.34±0.04 MPa to 1.41±0.25 MPa and 0.6±0.04 MPa (Fig. 2.4a & b). The maximum error of for the FE models compared to the

experimental measurements for mean and peak contact pressures were 23.8% for elbow 1 at 80N compression and -22.9 % for elbow 2 for 140N compression respectively.

Contact area

The computed contact areas using both FE-models ranged from 267.2±30 to 350.7±47 mm^2 whereas the experimentally measured areas ranged from 178±29 to 220±34.5 mm^2 across the loading conditions (Fig 2.4c).

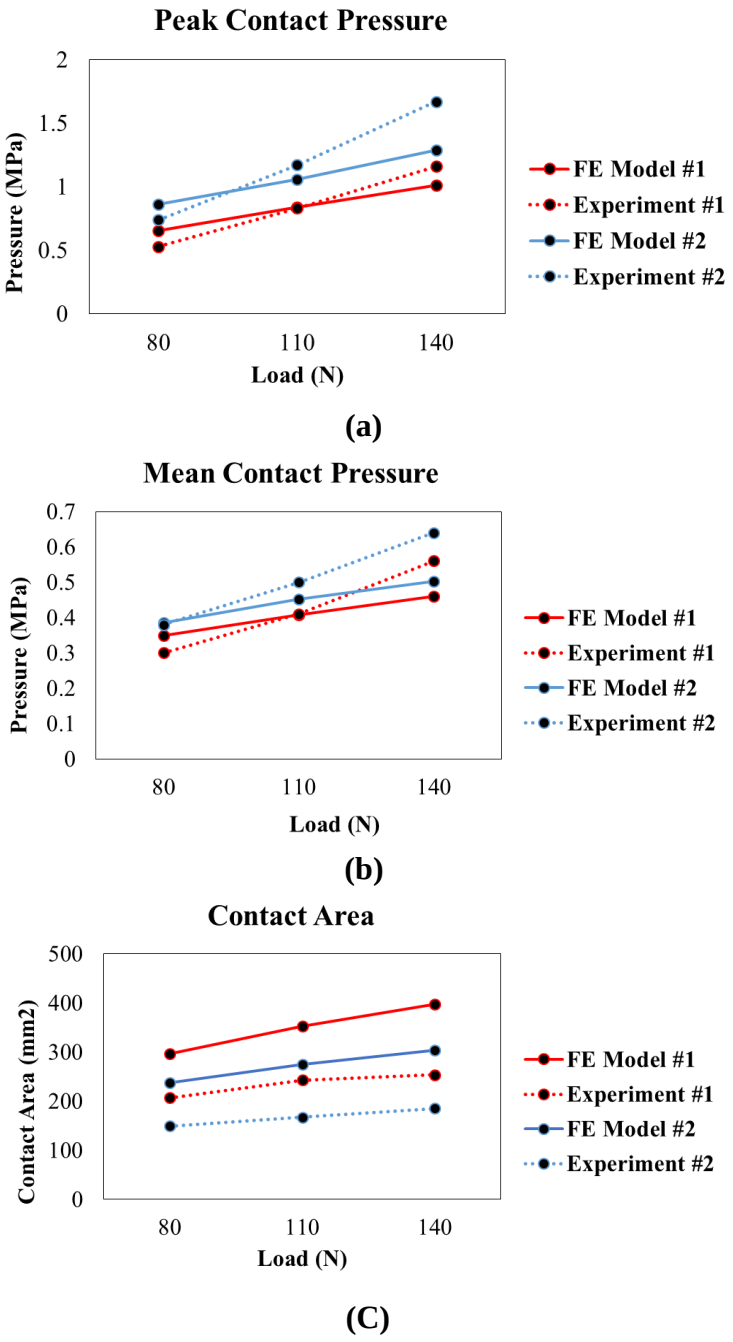

Figure 2.4. Peak contact pressure (a), mean contact pressure (b), and contact area (c) of the FE models and experimental measurements of two elbows versus the applied loads.

Parametric analysis

The parametric analysis shows that decreasing the Poisson's ratio from 0.49 to 0.43 causes a significant decrease in peak pressures, while changes in average pressure and contact area were less than 10% (Fig. 2.5a). Changing the Young's modulus did not have a remarkable effect (less than 6%) on the contact mechanics (Fig. 2.5b).

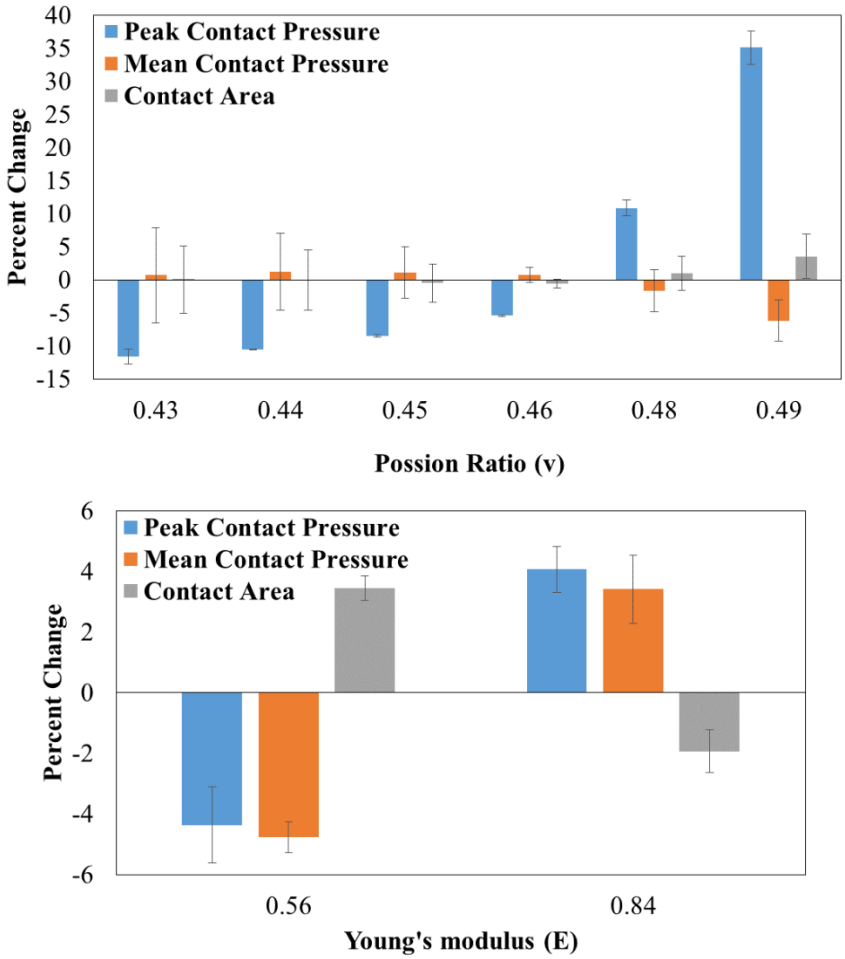

Figure 2.5. Percent changes in peak contact pressure, average contact pressure and contact area due to alterations in Possion ratio (a) and Young's modulus (b). Error bars specify standard deviations over the two finite element models.

2.4 Discussion

The primary purpose of this work was to develop FE models of the ulno-humeral joint and evaluate the models by direct measurements of their joint contact using a tactile pressure sensor across different static loading conditions. The sensitivity of the developed FE-models predictions to cartilage parameters was also investigated. The model predicted contact pressure distribution and contact pattern was in good agreement with the experimental measurements for the three loading cases. The average difference between the FE models and the experimental measurement in predicting the peak and mean contact were approximately 12% percent. Even though the contact areas predicted were larger than the experimentally measured areas, a similar trend was observed in both elbows as the applied load increased. The contact area increased posteriorly and laterally (Stormont, An, Morrey, & Chao, 1985). One possible explanation for this discrepancy could be the stiffness and sensitivity of the tactile sensor to measure the small contact pressures which would introduce an error in sensing the complete contact area.

Previous studies measured the contact areas between the elbow joint surfaces using different techniques, including cartilage staining, joint casting method, Fuji pressure film, and articular cartilage overlaps (Goel, Singh, & Bijlani, 1982; Kim & Carl Miller, 2016; Stormont, et al., 1985; R. Willing, Lapner, Lalone, King, & Johnson, 2014; R. T. Willing, et al., 2013). However, to our knowledge, there are no published experimental measurements of the contact pressure distribution within the ulno-humeral joint. Qualitatively, the predicted FE contact patterns were similar to the contact patterns measured with the pressure sensor. In both FE models and experimental measurements, the maximum contact pressures were located on the distal trochlea of the humerus. Overall, the FE-predicted mean and peak contact pressure

agreed well with experimental measurements. The FE-computed peak and mean contact pressure at 80N were higher than the experiment, while these values were less than the experimental measurements for 110N and 140N load. At higher loading condition, the stiffness of sensor can prevent it from conforming to the curvatures and surfaces of articular cartilage, thus measuring smaller contact areas and consequently larger pressures. Moreover, since at the higher loading the contact area over the articular cartilage was increased, it was possible that some regions of the load-bearing structures were placed physically outside the pressure sensor area and not recorded by the sensor matrix. Therefore, the pressure sensor recorded a higher mean and peak contact pressure but smaller contact area compered to FE models under the same load (Mootanah, et al., 2014). Inaccuracy of the pressure sensor in measuring the contact area by itself could be another reason in underestimating the contact area and consequently, overestimating the mean and peak contact pressure at higher loading scenarios (Drewniak, Crisco, Spenciner, & Fleming, 2007). Other factors such as ulno-humeral curvature which produces a preload on the sensor, and difference in calibration and joint temperature could lead to sensor errors (Agins, Harder, Lautenschlager, & Kudrna, 2003; TekscanWebsite; Wilharm, et al., 2013).

Even though the FE model's computed contact areas were not in a good agreement with the contact areas measured by the pressure sensor, they were consistent with previous studies that measured the contact area by casting which is a more reliable technique with small overestimating in measuring the contact area (Stormont, et al., 1985). The predicted numerical and experimental value of the total contact area of elbow joint (both ulno-humeral and humero-radial joints) at 20^{o} flexion angle under 80N axial load reported by Willing, et al. (2013) (R. T. Willing, et al., 2013) were 342 and 375 mm^2 respectively. They also indicated the contact

area on humerus joint was increased by increasing the flexion angle, while changing the contact area on radial cartilage is negligible when the elbow is flexed from 15 to 50 degrees(R. Willing, King, & Johnson, 2015). Chantelot, et al. (2008) (Chantelot et al., 2008) reported that the humero-radial articular cartilages experiences 6-25% of the total contact at full extension. By considering the above mentioned points, if the humero-radial contact area is subtracted from the total elbow joint's contact area reported by Willing, et al. (2013), then the measured numerical and experimental contact area on isolated ulno-humeral joint will be approximately 316±36mm^2 and 289±32 mm^2 respectively (R. T. Willing, et al., 2013). The FE-computed contact areas in this study for 80N axial load ranged from 237 to 297 mm^2. The small difference between the two studies can be attributed to how the cartilage was modeled. In our study, cartilage was modeled as a nearly incompressible material (v=0.47) while by Willing, et al. (2013) (R. T. Willing, et al., 2013) it was modeled as a compressible material (v=0.07). Furthermore, in this study the joint had only one degree of freedom along the long axis of humerus whereas they provided the translation and rotation about long axis of the forearm. Adding a rotational degree of freedom to the model could change the equilibrium position and consequently increase the contact area. Additionally, the radius and radial cartilage were not included in the current FE analysis. Finally, inherent specimens' variations can also affect the final results.

The cartilage Poisson's ratio variation did not have a significant effect on the predicted mean contact pressure and contact area (±6% and ±3.5% respectively). However, it had a great impact on the peak contact pressure. Increasing the Poisson's ratio from 0.43 to 0.47 increased the peak contact pressure from 0.84±0.13 to 0.95±0.14 MPa and almost no change in mean contact pressure (from 0.434±0.053 to 0.430±0.022 MPa), while increasing the Poisson's ratio

from 0.47 to 0.49 (nearly incompressible) caused a significant increase in peak contact pressure (from 0.95±0.14 to 1.29±0.21 MPa) and a minor change in mean contact pressure (from 0.43±0.02 to 0.40±0.01 MPa). This finding confirmed the previous study (A. E. Anderson, et al., 2008) and suggests that Poisson's ratio should be selected more critically for accurate prediction of peak contact pressure. Variation of Young's modulus did not have a significant effect on peak pressure predictions with variations less than 6% from the baseline case. A similar result has been reported in finite element studies performed on elbow and hip joints (A. E. Anderson, et al., 2008; Li, Stewart, Jin, Wilcox, & Fisher, 2013; R. T. Willing, et al., 2013).

The cartilage was modeled as a nearly incompressible hyperplastic constitutive material. This model is reliable for two conditions: First, when the cartilage reaches its equilibrium condition and the internal fluid is squeezed out, Second, when the cartilage is subjected to the instantaneous loading (Deneweth, Arruda, & McLean, 2015; Kazemi, Dabiri, & Li, 2013; Meng, et al., 2014). Since there is no fluid pressurization effect in both cases, the time-dependent response of the cartilage stress-strain is negligible, while its non-linearity responses is considerable (Korhonen et al., 2002). In this study, we assumed that the cartilage reached to its equilibrium condition after 10 minutes of applied constant load (Hosseini et al., 2010). Therefore, hyper elastic material with relatively high Poisson's ratio close to 0.5 were used to approximate the non-linearity and incompressibility behavior of the cartilage (Kazemi, et al., 2013). The effect of time-dependent contact behavior of cartilage will be studied in future work by incorporating a biphasic model for cartilages material in our FE models. Ligaments and joint capsule were not included in these FE models. Even though they might not significantly affect the contact behavior at static loading conditions, incorporating those structures in dynamic conditions may be necessary and will be considered in future work.

Applied load in this study does not necessarily replicate the physiological load applied on joint, and it's another limitation of the current study.

In conclusion, our approach in developing subject–specific FE models was reliable for studying the ulno-humeral joint contact pattern, contact area and contact pressure under static conditions. The two developed FE model predictions were in good agreement with experimental measurements taken with a tactile sensor placed in the joint and were consistent with previous studies. A parametric study on cartilage material properties was also conducted to assess the effect of uncertainty in model inputs to the model outputs. It indicated that selecting an appropriate value for cartilage material properties specifically Poisson's ratio is very important for predicting the contact pressure accurately. This study provides a framework for developing subject-specific FE models of the ulno-humeral joint and direct evaluation of their accuracy using tactile pressure sensors.

CHAPTER 3

CALIBRATING MULTIBODY ULNO-HUMERAL JOINT CARTILAGE USING A VALIDATED FINITE ELEMENT MODEL.

3.1 Introduction

Injury induced osteoarthritis of the elbow can cause severe pain, loss of mobility, and upper limb disability (Hildebrand, Patterson, & King, 1999; B.F. Morrey, 2000). A better understanding of elbow cartilage contact mechanics is essential in understanding the causes of cartilage degeneration, designing elbow joint prosthesis, and evaluation and development of appropriate treatment strategies. In vivo measurement of articular cartilage contact forces and joint loading is not possible, necessitating the use of computational models.

Computational modeling has become a very popular tool for predicting and characterizing the function of complex musculoskeletal systems, for improving orthopeadic interventions, and in medical device development. Accurate computational models can predict the behavior of various physiologic parameters or medical device components simultaneously and quantitatively. They also mitigate the need for expensive experimental tests and large sample sizes in physical test and clinical trials. Furthermore, after validation, models can be employed in parametric and optimization studies of various injuries, disorders, evaluations of new surgical techniques or implantations, and to predict in-vivo joint loads (J.P. Fisk, 2007; Spratley & Wayne, 2011).

Finite element (FE) modeling and multibody (MB) dynamics are the two main mathematically formulated approaches employed in structural computational modeling. FE models are typically used to predict stress, strain, and deformation of isolated joints, tissues,

and prosthesis under physiologically or experimentally applied loads or displacements. Even though FE models have many advantages, they also have certain drawbacks including, being computationally intensive due to large number of unknowns in the associated system of equations, and inability to do concurrent simulation at the body level. On the other hand, when stress or strain computations are unnecessary, a dynamic computational model (multibody) in which muscle, ligament, and articular surface contact forces are predicted concurrently would be an ideal and efficient tool for body-level musculoskeletal movement simulations (J.P. Fisk, 2007; Kia, Stylianou, & Guess, 2014; Stylianou, Guess, & Cook, 2012). Multibody models use rigid body dynamics, hence soft tissue deformations cannot be predicted.

Several studies developed anatomically correct computational multibody models of the elbow and forearm (J.P. Fisk, 2007; J. P. Fisk & Wayne, 2009; M. Rahman, Cil, A., Johnson, M., Lu, Y., Guess, T.M., 2014; Spratley & Wayne, 2011). In these studies, either the cartilage was not included (J.P. Fisk, 2007; J. P. Fisk & Wayne, 2009; Spratley & Wayne, 2011) or the contact model was simulated using a single point contact (M. Rahman, Cil, A., Johnson, M., Lu, Y., Guess, T.M., 2014). Articular cartilage contact force prediction is one of the most important and challenging problems encountered in musculoskeletal modeling because of its dependency on many factors including geometry of the contact bodies, material, and constitutive laws for defining the interaction between the bodies of a dynamic systems. The behavior of colliding bodies in the multibody framework is usually modeled using compliant contact. The compliant contact model also known as deformable contact or penalty model, is a function of indention and compliance of the contacting surfaces (Machado, Moreira, Flores, & Lankarani, 2012). Due to its simplicity and efficiency, it has been used in many multibody models and studies (Flores, Machado, Silva, & Martins, 2011; Gonthier, McPhee, Lange, &

Piedboeuf, 2004).The original compliant contact model is a pure elastic contact based on Hertz law, in which the contact force is a nonlinear power function of the indentation. This model does not include the energy dissipation process that characterizes the contact–impact events. An internal damping term was added to the pure elastic contact model to accommodate energy dissipation (Hunt & Crossley, 1975). The proposed contact model is a well improved and implementable contact model which has been used in many studies (R. W. G. Anderson, Long, & Serre, 2009; Guess, Liu, Bhashyam, & Thiagarajan, 2013; Kia et al., 2016; Moreira, Flores, & Silva, 2012; Silva, Silva, & Martins, 2010; Stylianou, Guess, & Kia, 2013).

Since, there is a large deformation in the contact zone during the conformal contact, prediction of the contact area and contact distribution is not feasible through contact model used in the multibody models. Elastic foundation theory is an efficient approach to overcome this limitation. In the elastic foundation model, the body surfaces are represented by polygon meshes and a set of springs spreads over the contact surface (bed of springs). The springs represent the elastic layer of contact surfaces which is based on the composed elastic modulus of two bodies' surfaces (Bei & Fregly, 2004; Blankevoort, Kuiper, Huiskes, & Grootenboer, 1991; Mukras, Kim, Mauntler, Schmitz, & Sawyer, 2010; Perez-Gonzalez et al., 2008). Guess et al (Guess, et al., 2013) employed similar approach to model the interaction between tibia and femoral cartilage in a 3-dimensional knee multibody model. The tibial cartilage was discretized and a dissipative compliant contact formulation between each discretized rigid element and the contacting femoral cartilage was defined to model the interaction between knee joint articulating surfaces (Guess, et al., 2013).

Correct choice of the contact parameters such as equivalent stiffness, damping coefficient, and the nonlinearity of the indentation are the main challenges in using contact

models in the multibody framework. To address this difficulty, Guess et al (Guess, et al., 2013) estimated these values based on a finite element model and optimization approach. A single cadaver model was used in the FE optimization procedure and the transferability of the predicted contact parameters to other specimens was not evaluated. Recently, Rahman et al. (M. Rahman, Cil, Bogener, & Stylianou, 2016; M. Rahman, Cil, & Stylianou, 2016) employed the same method in the elbow joint which has different geometrical congruency compared to tibial cartilage. The contact parameters used were based on elastic foundation theory, however, they were not validated through direct cadaveric measurements.

The main objectives of this study were: (i) to calibrate the humero-ulna articular cartilage contact parameters to validated FE models, (ii) test the validity of the implemented method for different loading conditions, (iii) assess the effect of specimen variability on the proposed articular cartilage contact parameters calibration method.

3.2 Methods

Experiment

Contact pressure within two non-pathological cadaveric elbow joints (from a 69 a year old man (left and right elbows) was measured using a tactile pressure sensor (Model-4201, Tekscan Inc., Boston, MA, USA) for different axial loads. The cadaveric specimens were prepared by removing all soft tissue around the elbow joints while the capsule and ligaments were kept intact. Three localizers, filled with mustard, were rigidly attached to each bone segments. The mustard tubes are visible in magnetic resonance imaging (MRI) and used for registering the experimental position of the bone segments to the MRI derived bone geometries.

The pressure sensor was calibrated using 3 point calibration at approximate of 25%, 75%, and 125% of the maximum axial expected load, sealed between two layers of Tegaderm adhesive waterproof transparent dressing (3M, NexcareTM), and then positioned inside the elbow joint by inserting the sensor anteriorly into the joint and using sutures to pull the sensor back from the posterior side. The humerus, ulna and radius were sectioned midshaft and potted into two cylindrical cups at 20 flexion angle (Fig. 3.1a). The cups were attached to a bi-axial Instron 8821 (Instron, Norwood, MA, USA) mechanical testing machine with attached load cell of 300N. A point cloud was collected at the initial position using an Optotrack rigid probe (NDI, Waterloo, Ontario, Canada). This data was used to align the geometries later in the computational model. The humerus was subjected to three different axial loads: 80N, 110N, and 140N with a rate of 1mm/min and maintained for 10 min to allow viscoelastic deformation of cartilage to become constant (Ateshian, et al., 2015). Contact pressure data was recorded during the experiment and used for evaluation of the finite element models.

Geometry preparation

The MRI sequences (image resolution of 256 x 232, slice thickness 0.5mm, and spacing between slices 0.1mm) were used to generate 3D models of bones, cartilage and localizers. The 3D geometries were generated in two steps using image processing software (Mimics, Materialise, Inc., Leuven, Belgium). First, auto thresholding and manual segmentation were implemented to get the bones and cartilages overlapped with bones geometries. Then, boolean subtraction was used to isolate the cartilage geometries from the bones. The geometries were wrapped and imported into Meshlab (Visual Computing Lab - ISTI – CNR) for smoothing the surfaces and noise reduction.

Finite element model

The 3D geometries were converted into 3D tetrahedral elements and imported into FEBio Preview (version 1.7; mrl.sci.utah.edu/software.php) for defining boundary conditions identical to the physical test. The approximate element edge size of the bone and cartilage meshes were 2 and 1 mm respectively. Since the Young's modulus of bone is much higher than cartilage, the bones were considered as rigid bodies and the cartilages were modeled using an incompressible Moony-Rivlin hyperplastic material (E=0.7 MPa, v=0.47) (Schenck, et al., 1994; R. T. Willing, et al., 2013). Interactions between cartilage-cartilage and cartilage-bones were defined as friction-less surface to surface contact and tie contact respectively (Erdemir, 2016). Load of 80N, 110N, and 140N were applied on the humerus along the long axis of the bone while the ulna was fully constrained (Fig. 3.1b). FEBio software was used for solving the mathematical equations numerically. The contact pressure distribution (third principal stress) across the articular cartilage surface elements, its maximum value, and the contact area were computed and used for comparison against the experiment. Subsequently the peak pressure (average of 6 element) was used as a reference for tuning the multibody contact parameters.

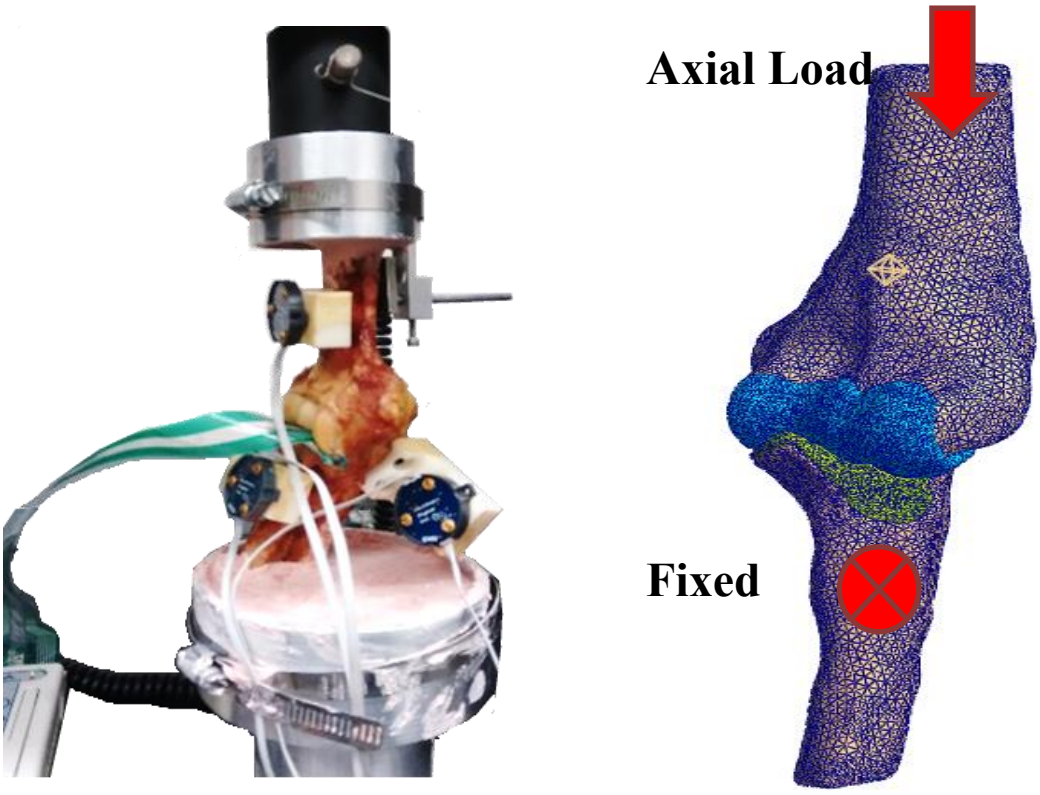

Figure 3. 1. Positioned elbow in experiment (a) and Finite Element (b).

Multibody model

Multibody models were created in ADAMS (MSC Software Corporation, Santa Ana, CA) by importing the bone and cartilage geometries as STL files (Fig. 3.2a). A custom macro was written in ADAMS to automatically divide the humerus cartilage into discrete hexahedral elements of two different sizes and connect each discretized element to the humerus surface using a fixed joint (Fig. 3.2b). The macro also defined a deformable contact constraint with no friction using modified Hertzian contact law (Hunt & Crossley, 1975) between each created humerus cartilage element and ulna cartilage geometry:

$$F_c = K_c\delta^n + B_c(\delta)\dot{\delta} \dots\dots\dots (1)$$

Where K_c is the contact stiffness, δ is the interpenetration of the geometries, n nonlinear force exponent, $B_c(\delta)$ is a damping coefficient, and $\dot{\delta}$ is the velocity of interpenetration. The ulnar cartilage geometry was attached rigidly to the bone surface using fixed joints. Identical boundary and loading conditions to the FE models were applied to the multibody models. The ulna was fixed in all degrees of freedom while the humerus could move along its proximal distal axis. An axial constant load was applied to the humerus and the simulation was conducted for 5 sec with the step size of 0.01 s. Contact force on each element as well as their coordinate positions were exported to create pressure distribution on the opened articular cartilage in 2D.

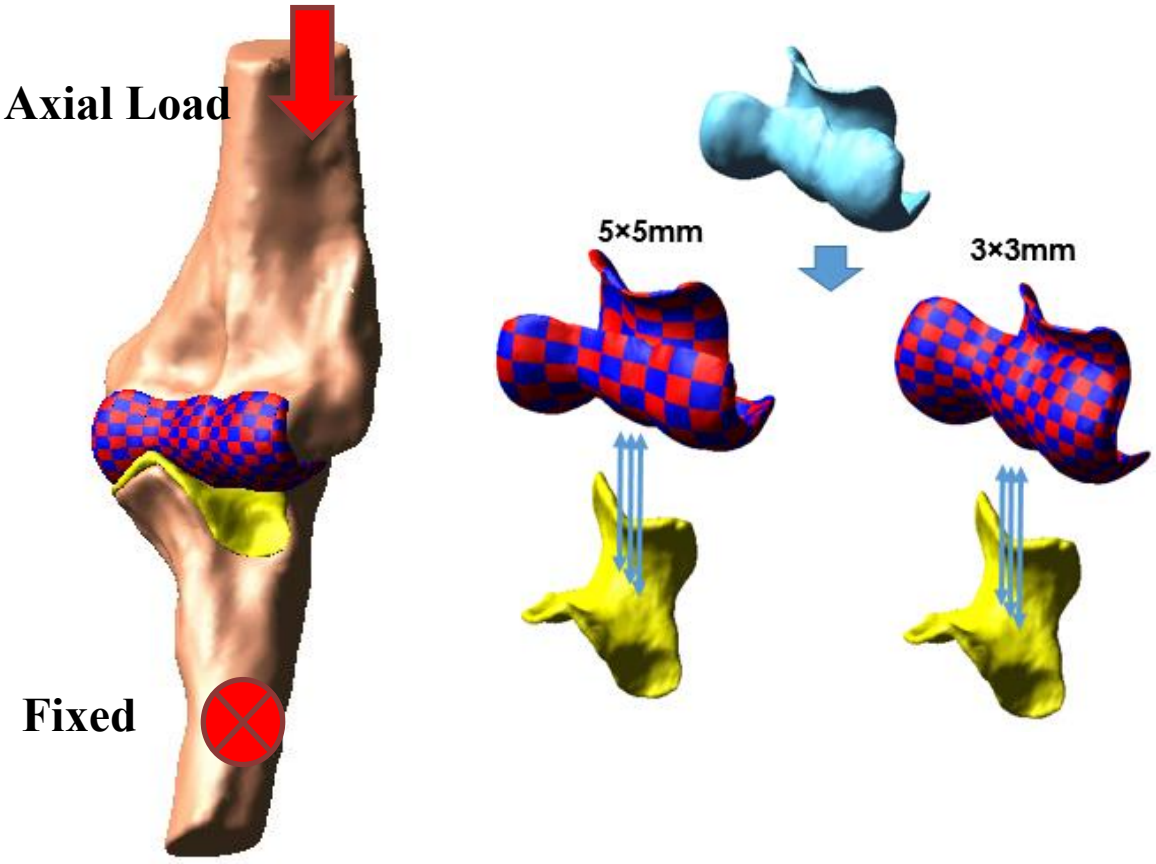

(a) **(b)**

Figure 3.2. Multibody model of ulno-humeral joint with discretized articular cartilage (a), discretized rigid body of humerus cartilage in two different sizes (5×5 mm and 3×3 mm) interacting to ulna cartilage through contact force.

Optimization

The effect of element size on contact mechanics was explored using two different element sizes of 3x3mm, and 5x5mm under 110N loading condition. The contact pressure in the multibody frame work was calculated by dividing the contact force by the contacting surface area of each element. The contact parameters and discretized element size were optimized such that the maximum contact pressure of the elbow joint matched with the experimentally validated finite element model. The design of experiment and optimization

approach in ADAMS/insight was utilized to implement the optimization process. In order to evaluate our optimized values for other loading conditions, the contact pressure (maximum and mean) and contact area were calculated for 80N and 140N and compared with their corresponding values measured from FE model. Contact area was calculated using multiplying the number of discrete element capturing pressure higher than threshold pressure (0.11MPa) by cross section area of each elements, 3×3 (9mm^2) and 5×5 (25mm^2).

3.3 Results

The optimized contact parameters were varied among two elbows. Damping coefficient values were almost consistent for all cases before and after optimization while the stiffness and force exponent are much more sensitive to the geometry and discrete sizes. The maximum predicted contact pressure error was reduced by approximately 86% and 100% for elbow #1 and elbow #2 respectively after the optimization (**Table 3.1 & 3.2**). The model with 3×3 element size had significantly less error compared to 5×5 element size.

Table 3.1. Initial, optimum contact parameters, their corresponding maximum contact pressure, and error relative to FEA values for elbow #1.

Elbow #1				
Parameter	**5 × 5**		**3 × 3**	
	Initial value	**Optimum value**	**Initial value**	**Optimum value**
K_c	400	323.7	200	39.154
B_c	5	5	5	5.0791
n	4	3.1434	4	3.0513
Max pressure (MPa)	0.9084	0.8395	1.1190	0.8403
MB error relative to FEA (MPa)	0.0261	-0.0004	0.2367	0.0004

Table 3.2. Initial, optimum contact parameters, their corresponding maximum contact pressure, and error relative to FEA values for elbow #2

Elbow #2				
Parameter	**5 × 5**		**3 × 3**	
	Initial value	**Optimum value**	**Initial value**	**Optimum value**
K_c	400	546.51	200	197.55
B_c	5	5	5	5
n	4	6.4565	4	3.8219
Max pressure (MPa)	0.8524	1.0380	1.0700	1.0560
MB error relative to FEA (MPa)	0.2000	0.0202	0.0120	0.0020

After using the optimized contact parameters, the predicted maximum contact pressure for the multibody models were consistent with the corresponding FE models for loading conditions of 80N and 140N. It confirmed the validity and replicability of the optimization approach for a range of loading conditions (Fig 3.3a & b). The maximum contact pressure error between the FE and multibdy models was less than 9% and occurred for elbow #2 with 5×5 discrete size under 80N loading.

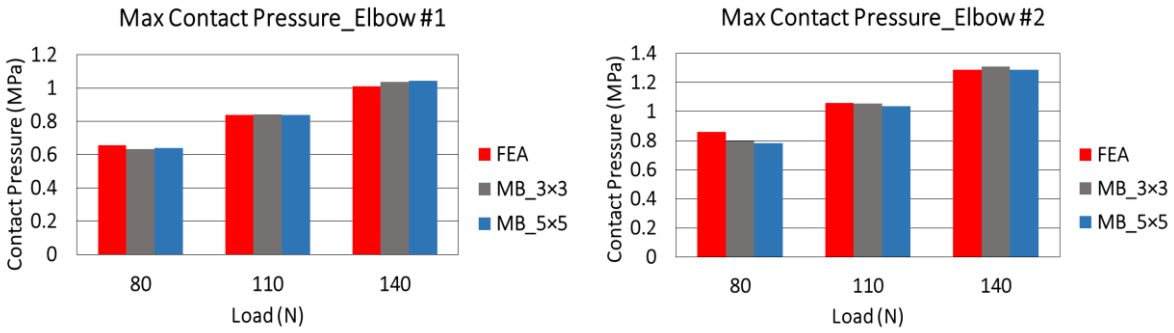

(a) **(b)**

Figure 3.3. Maximum contact pressure predicted by FE and optimized MB models for 80N, 110N, and 140N loading condition.

The resulting contact pressure distribution and contact patches in the MB models were consistent with the FE models for different loading conditions and for both elbows after

optimization (Fig 3.4 & 3.5). The MB with 3×3 grid size discrete cartilage predicted the contact pressure distribution more accurately compared to 5 x5 element size, especially when the geometries contained high curvature.

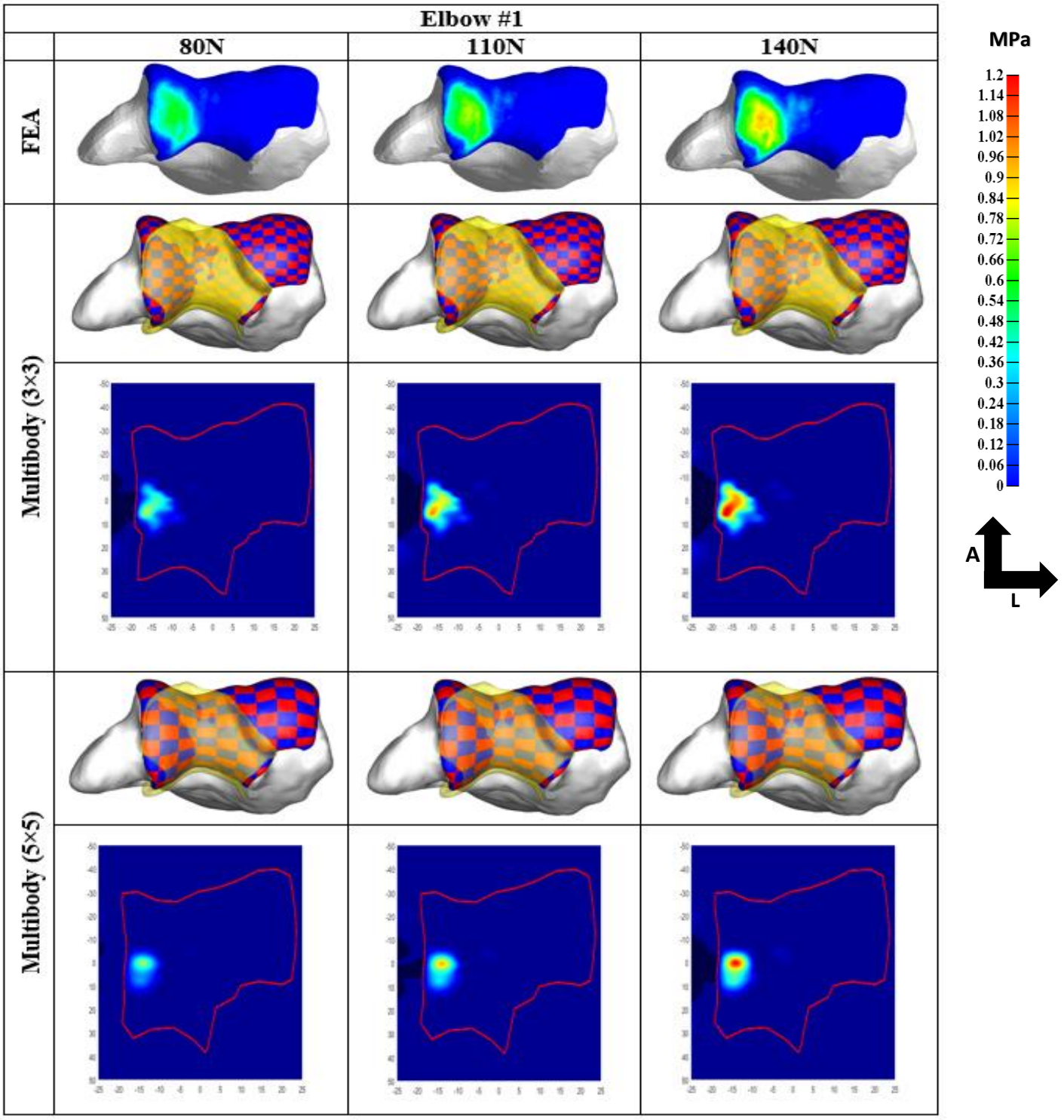

Figure 3.4. Contact pressure distribution and contact patch of FEA and MB models for different loading conditions for elbow #1.

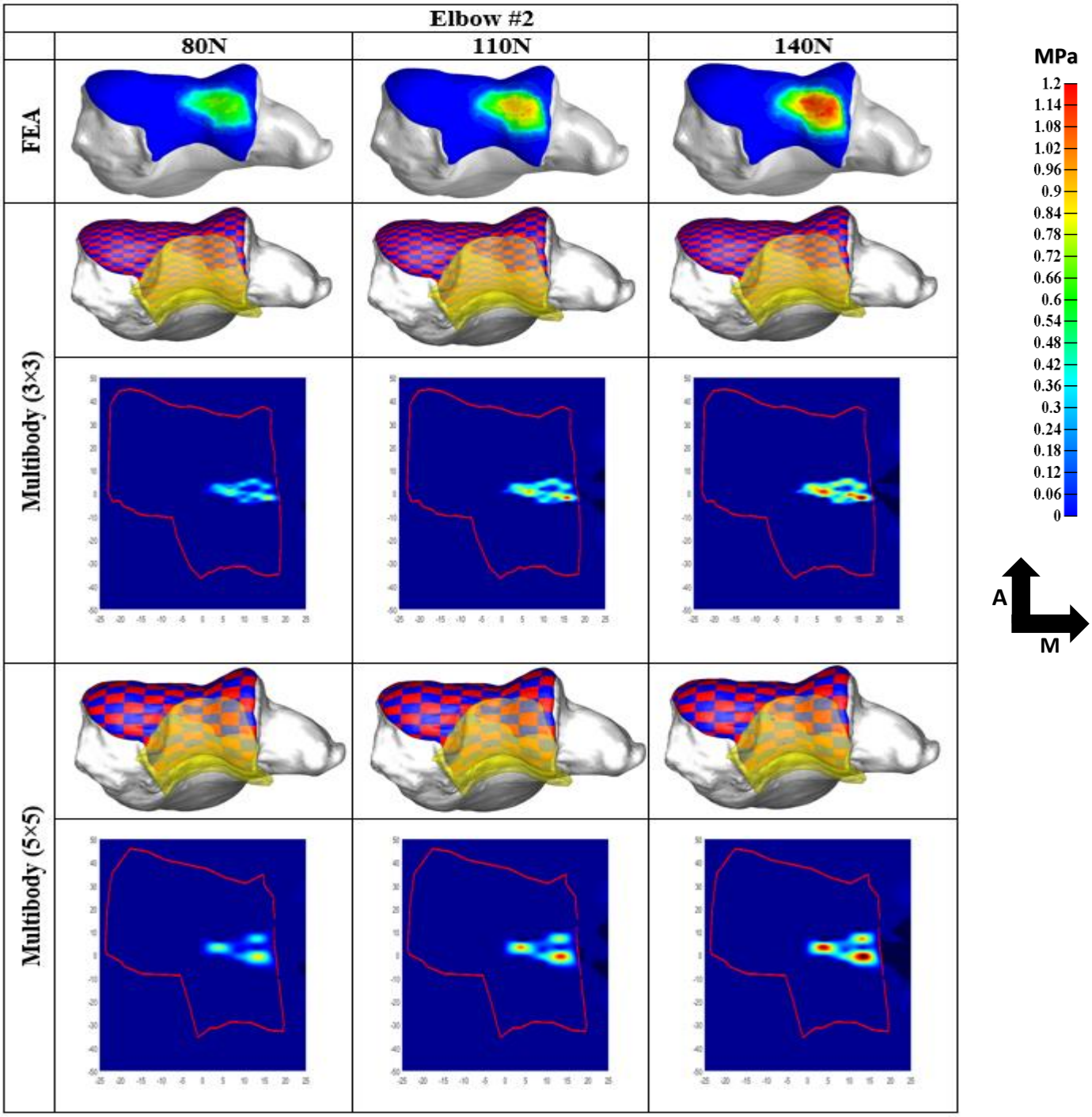

Figure 3.5. Contact pressure distribution and contact patch of FE and MB models (3×3 and 5×5) for different loading conditions for elbow #2.

Similar to the FE models, the average contact pressure and contact area of the optimized MB models were increased with increasing applied load. Among the two elbows, the maximum error of average pressure between MB and FE models was 0.12 MPa and observed for elbow #2 with 5×5 discrete element size under 140N load. The maximum contact area error between MB and FE model was 248 mm^2 and observed for elbow #1 with 5×5 element size under 140N load. Overall, the 3×3 discrete size captured the average contact pressure and contact area more accurately with the FEA model compared to 5×5 discrete size.

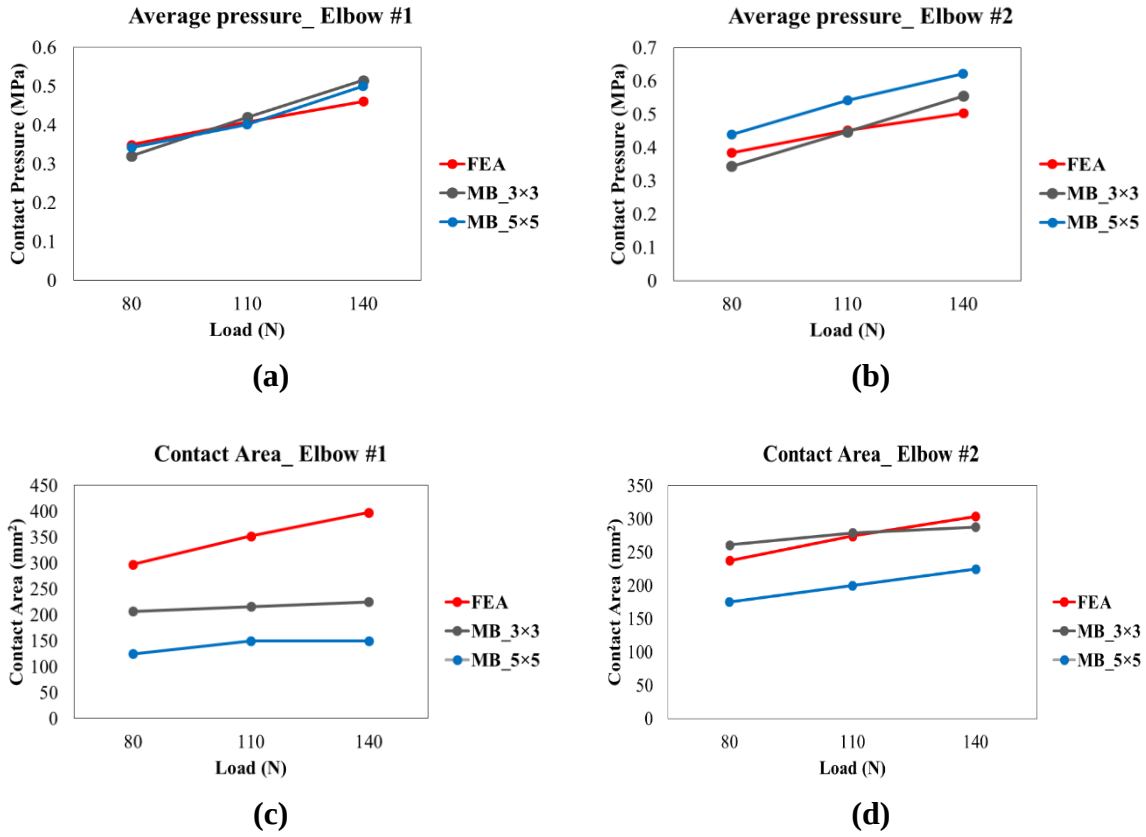

Figure 3.6. Average contact pressure and contact area of FE and MB models (3×3 and 5×5) for different loading conditions for elbow #1 and #2.

3.4 Discussion

Accurate choice of contact models and their parameters has always been a challenging issue in contact mechanics in the multibody framework. Converting a rigid body geometry to multiple discrete elements and defining appropriate contact equations and parameters for each discrete element can be a reliable approach to solve this difficulties and can be employed in different joint with different geometry congruency (Guess, et al., 2013; M. Rahman, Cil, & Stylianou, 2016; Stylianou, et al., 2012). This study aims to predict the contact mechanics of the highly curved geometry of the elbow joint articulation in the multibody frame work using discretized humerus cartilage (a bed of spring and damper) paired with a FE based optimization approach. The contact parameters of the discretized cartilage were optimized to match the maximum contact pressure predicted in the FE models, and the validity of the discretization technique was tested under two different loading conditions. The effect of discrete rigid body size was also investigated as an important factor in contact mechanics of multibody models.

Predicted maximum contact pressure of multibody models with tuned contact parameters were in good agreement with FE model predictions not only under the optimization loading, but also under the two other loading conditions, contact patch of multibody models were similar to FE models. In both elbows, the maximum contact pressure error between FE and multibody models for both discrete sizes ranged from 9% to 0.05%. Computed areas occurred in the trochlea and expanded medially to the middle edge of the trochlea. Similar to the FE model for elbow 1, the corresponding MB models predicted more contact area in the posterior region of humerus cartilage. Their pressure distributions were also well matched with FE predictions. The peak pressure were located on the most medial distal region of the trochlea and it gradually decreased posteriorly and laterally. Due to geometries congruency of elbow

#2, the peak pressure was more scattered over the cartilage surface compared to elbow #1. This pattern was observed in both FE and MB models. The mean contact pressure and contact area predicted by the multibody models increased by increasing the applied loads. The maximum error of mean pressure between FE and MB models was 0.12 MPa while the maximum contact area error was 247.65 mm^2.The main reason for the higher discrepancy in contact area predictions can be attributed to the method used to calculate the contact area. In both MB models, the number of discrete elements which underwent a pressure higher than 0.11 MPa were considered for contact areas calculation. For elbow #1, especially with 5×5 size, elements located in high curvature areas were experiencing contact pressure below the selected threshold, therefore the contact areas were omitted. However, for elbow #2, since the elements in contact were not in high curvature regions, more elements experienced contact pressure above the threshold, thus reducing the error between FE and MB models contact area predictions.

Overall, the multibody models with discrete element size 3×3 predicted the average contact pressure and contact area more closely with FEA model. The maximum errors of average contact pressure and contact area in 5×5 were 0.1186 MPa and 247.65 mm^2 respectively while these values were 0.054 MPa and 172.65 mm^2 in 3×3. Since, 3×3 discrete sizes are smaller than 5×5, they could conform to geometric variations better. Since the elbow joint cartilage has high curvature areas, correct prediction of contact pressure distribution was very sensitive to discretized element sizes and the 3×3 grid performed better in prediction of regional contact pressure distribution. A similar result has been reported for a knee joints studies and it suggested that 3×3 elements size has better accuracy for predicting contact characteristics (Guess, et al., 2013; Stylianou, et al., 2012).

Interestingly, this study suggests that the optimizing contact parameters based on FE models can vary among elbow joints. This difference can be explained by geometrical differences in the ulno-humeral joints, the optimization pressure, and the number of humerus elements in contact with ulna during the static optimization. Under the same loading condition, the peak pressure and the number of element in contact for elbow #1 was smaller and higher than the elbow #2 respectively. In elbow #1, almost 63 elements with 3×3 size and 25 elements with 5×5 size are in contact under the 110N load while in elbow #2, 43 elements with 3×3 size and 15 elements of 5×5 size are in contact with ulna cartilage. More elements in contact with ulna cartilage, will result in smaller values computed for the equivalent stiffness and force exponent.

The proposed method for establishing the appropriate contact parameters in a multibody model of the ulno-humeral joint is reliable on a subject specific basis and could be applicable in other joints. Since the finite element models are computationally intensive and cannot be used for body level dynamic simulation, multibody analysis is an efficient alternative. The contact mechanics predicted by MB models with two discrete sizes and optimized contact parameters were well matched with FE models which were validated against experimental data collected from tactile sensor. The models with optimized contact parameters also indicated a good response under other loading conditions. Moreover, the effect of discrete size and geometrical variability of the joint on contact mechanics was explored. It revealed that the smaller discrete size predicts contact characteristics more accurately, a result that is consistent with previous study(Guess, et al., 2013). However, the same study showed that reducing the element size smaller than 3×3 increased the computation time without significant improvements in contact mechanics predictions (Guess, et al., 2013). More importantly, we

demonstrate that that optimized contact parameters can be different not only among different joints, but also among different specimens and optimization conditions. Obviously, in order improve contact predictions, separate contact optimization should be done for each subject; however, this study gives approximate values for contact parameters and discrete element sizes that can be useful for multibody elbow joint modeling. Including more specimens and evaluating optimized contact parameters under dynamic conditions should also be performed as a future step to increase the credibility of the multibody models and computed contact parameters.

CHAPTER 4

CONCLUSION

The presented manuscript describes two separate studies on contact mechanics of the ulno-humeral joint, the main joint in the elbow. Computational modeling techniques including finite element and multibody as well as cadaveric experiments were employed to investigate joint contact characteristics under static loading conditions. The results from the FE and multibody models can be used for improving computational models of the elbow join.

In chapter 2, the primary objectives of the ulno-humeral elbow joint FE modeling were to 1) developing subject specific finite element models of the ulno-humeral joint, 2) direct comparison of FE-computed contact pressure distribution against experimental measurements taken with a tactile sensor, and 3) investigating the model's sensitivity to the cartilage mechanical properties.

In summary, in this study a tactile pressure sensor was used to measure the contact pressure distribution within the ulno-humeral joint of two cadaver specimens at 20 degree flexion angle across three different axial loads of 80N, 110N, and 140N. Corresponding 3D finite element (FE) models of the same elbows were constructed from magnetic resonance imaging (MRI) and the contact analysis was performed for each specimen with boundary and loading conditions identical to the experiment applied to the models. Direct comparison between FE results and experimental measurement was conducted for the validation of the FE models and sensitivity analysis was employed for assessing the effect of the cartilage parameters on the model's outputs. The results showed a good agreement between the FE models and the experiments in terms of contact characteristics. The sensitivity analysis demonstrated that outcomes of the model, particularly peak contact pressure is more sensitive

to the Poisson's ratio rather than to the young's modulus under static conditions. This result suggests that selection of Poisson's ratio is very critical for accurate prediction of contact mechanics within the ulno-humeral joint.

In chapter 3, the primary objectives of the ulno-humeral elbow joint FE modeling were to 1) calibrate the ulno-humeal articular cartilage contact parameters to validated FE models, 2) test the validity of the implemented method for different loading conditions, and 3) assess the effect of specimen variability on the proposed articular cartilage contact parameters calibration method.

In summary, two subject specific multibody models of ulno-humeral joint were developed in MD Adams. These models contained discretized humerus cartilage interacting with the ulna cartilage through a deformable contact which allowed direct measurement of contact pressures distribution and contact area. Parameters for deformable contact were optimized by matching the maximum predicted contact pressure in multibody models with their corresponding FE solutions under 110N axial loading condition. The validation of FE solution were presented in the chapter 2. The validity of optimized contact parameters and employed approach were evaluated under two other loading conditions of 80N, and 140N. In addition, the effect of discretized element size on the contact prediction was also addressed.

In this study, the ulno-humeral multibody models with FE optimized parameters predicted the contact mechanics including peak and average contact pressure, and contact area more accurately for different loading conditions. Smaller discrete sizes showed a better prediction especially on highly curvature regions. Moreover, it was found that the optimized contact parameters were different between the two elbows. This indicates that optimized contact parameters can be different not only among different joints, but also among different

specimens and optimization conditions. Therefore, in order to improve contact predictions, separate contact optimization should be performed for each subject.

Overall, this study provided a reliable methodology for correct prediction of joint contact characteristics in multibody framework where body level simulations are important. This methodology can be applicable not only in any other natural joints but also it can be more functional in simulations including joint prosthesis. Future steps for this study are: 1) increasing the samples, 2) improving FE model by adding ligaments, radius and radial cartilage, more advance articular cartilages like biphasic, 3) evaluating the optimization method for dynamic conditions like flexion-extension. Performing concurrent multibody, finite element, and artificial intelligence to predict the stress, strains, deformation, and wear within body level and multibody simulation or using flex body for cartilage are other worthwhile topics need to be explored in the future studies.

REFERENCES

Agins, H. J., Harder, V. S., Lautenschlager, E. P., & Kudrna, J. C. (2003). Effects of sterilization on the Tekscan digital pressure sensor. *Med Eng Phys, 25*(9), 775-780. doi: S135045330300119X

Anderson, A. E., Ellis, B. J., Maas, S. A., Peters, C. L., & Weiss, J. A. (2008). Validation of finite element predictions of cartilage contact pressure in the human hip joint. *J Biomech Eng, 130*(5), 051008. doi: 10.1115/1.2953472

Anderson, R. W. G., Long, A. D., & Serre, T. (2009). Phenomenological continuous contact-impact modelling for multibody simulations of pedestrian-vehicle contact interactions based on experimental data. *Nonlinear Dynamics, 58*(1-2), 199-208. doi: 10.1007/s11071-009-9471-6

Ateshian, G. A., Henak, C. R., & Weiss, J. A. (2015). Toward patient-specific articular contact mechanics. *J Biomech, 48*(5), 779-786. doi: 10.1016/j.jbiomech.2014.12.020

Bei, Y., & Fregly, B. J. (2004). Multibody dynamic simulation of knee contact mechanics. *Med Eng Phys, 26*(9), 777-789. doi: 10.1016/j.medengphy.2004.07.004

Blankevoort, L., Kuiper, J. H., Huiskes, R., & Grootenboer, H. J. (1991). Articular contact in a three-dimensional model of the knee. *J Biomech, 24*(11), 1019-1031.

Bryce, C. D., & Armstrong, A. D. (2008). Anatomy and biomechanics of the elbow. *Orthop Clin North Am, 39*(2), 141-154, v. doi: 10.1016/j.ocl.2007.12.001

Chantelot, C., Wavreille, G., Dos Remedios, C., Landejerit, B., Fontaine, C., & Hildebrand, H. (2008). Intra-articular compressive stress of the elbow joint in extension: an experimental study using Fuji films. *Surg Radiol Anat, 30*(2), 103-111. doi: 10.1007/s00276-007-0297-y

Dekel, S., & Weissman, S. L. (1978). Joint changes after overuse and peak overloading of rabbit knees in vivo. *Acta Orthop Scand, 49*(6), 519-528.

Deneweth, J. M., Arruda, E. M., & McLean, S. G. (2015). Hyperelastic modeling of location-dependent human distal femoral cartilage mechanics. *International Journal of Non-Linear Mechanics, 68*, 146-156. doi: 10.1016/j.ijnonlinmec.2014.06.013

Drewniak, E. I., Crisco, J. J., Spenciner, D. B., & Fleming, B. C. (2007). Accuracy of circular contact area measurements with thin-film pressure sensors. *J Biomech, 40*(11), 2569-2572. doi: S0021-9290(06)00480-510.1016/j.jbiomech.2006.12.002

Erdemir, A. (2016). Open knee: open source modeling and simulation in knee biomechanics. *J Knee Surg, 29*(2), 107-116. doi: 10.1055/s-0035-1564600

Fisk, J. P. (2007). Development and validation of a computational musculoskeletal model of the elbow joint. Virginia Commonwealth University. Richmond, Virginia

Fisk, J. P., & Wayne, J. S. (2009). Development and validation of a computational musculoskeletal model of the elbow and forearm. *Ann Biomed Eng, 37*(4), 803-812. doi: 10.1007/s10439-009-9637-x

Flores, P., Machado, M., Silva, M. T., & Martins, J. M. (2011). On the continuous contact force models for soft materials in multibody dynamics. *Multibody System Dynamics, 25*(3), 357-375. doi: 10.1007/s11044-010-9237-4

Goel, V. K., Singh, D., & Bijlani, V. (1982). Contact areas in human elbow joints. *J Biomech Eng, 104*(3), 169-175.

Gonthier, Y., McPhee, J., Lange, C., & Piedboeuf, J. C. (2004). A regularized contact model with asymmetric damping and dwell-time dependent friction. *Multibody System Dynamics, 11*(3), 209-233. doi: Doi 10.1023/B:Mubo.0000029392.21648.Bc

Guess, T. M., Liu, H., Bhashyam, S., & Thiagarajan, G. (2013). A multibody knee model with discrete cartilage prediction of tibio-femoral contact mechanics. *Comput Methods Biomech Biomed Engin, 16*(3), 256-270. doi: 10.1080/10255842.2011.617004

Hamby, D. M. (1995). A comparison of sensitivity analysis techniques. *Health Phys, 68*(2), 195-204.

Harris, M. D., Anderson, A. E., Henak, C. R., Ellis, B. J., Peters, C. L., & Weiss, J. A. (2012). Finite element prediction of cartilage contact stresses in normal human hips. *J Orthop Res, 30*(7), 1133-1139. doi: 10.1002/jor.22040

Hildebrand, K. A., Patterson, S. D., & King, G. J. (1999). Acute elbow dislocations: simple and complex. *Orthop Clin North Am, 30*(1), 63-79.

Hosseini, A., Van de Velde, S. K., Kozanek, M., Gill, T. J., Grodzinsky, A. J., Rubash, H. E., & Li, G. (2010). In-vivo time-dependent articular cartilage contact behavior of the tibiofemoral joint. *Osteoarthritis Cartilage, 18*(7), 909-916. doi: 10.1016/j.joca.2010.04.011

Hunt, K. H., & Crossley, F. R. E. (1975). Coefficient of restitution interpreted as damping in vibroimpact. *Journal of Applied Mechanics, 42*(2), 6. doi: 10.1115/1.3423596

Kazemi, M., Dabiri, Y., & Li, L. P. (2013). Recent advances in computational mechanics of the human knee joint. *Comput Math Methods Med, 2013*, 718423. doi: 10.1155/2013/718423

Kia, M., Schafer, K., Lipman, J., Cross, M., Mayman, D., Pearle, A., Imhauser, C. (2016). A multibody knee model corroborates subject-specific experimental measurements of low ligament forces and kinematic coupling during passive flexion. *J Biomech Eng, 138*(5), 051010. doi: 10.1115/1.4032850

Kia, M., Stylianou, A. P., & Guess, T. M. (2014). Evaluation of a musculoskeletal model with prosthetic knee through six experimental gait trials. *Med Eng Phys, 36*(3), 335-344. doi: 10.1016/j.medengphy.2013.12.007

Kiapour, A., Kiapour, A. M., Kaul, V., Quatman, C. E., Wordeman, S. C., Hewett, T. E., Goel, V. K. (2014). Finite element model of the knee for investigation of injury mechanisms: development and validation. *J Biomech Eng, 136*(1), 011002. doi: 10.1115/1.4025692

Kim, S., & Carl Miller, M. (2016). Validation of a finite element humeroradial joint model of contact pressure using fuji pressure sensitive film. *J Biomech Eng, 138*(1). doi: 10.1115/1.4031976

Korhonen, R. K., Laasanen, M. S., Toyras, J., Rieppo, J., Hirvonen, J., Helminen, H. J., & Jurvelin, J. S. (2002). Comparison of the equilibrium response of articular cartilage in unconfined compression, confined compression and indentation. *J Biomech, 35*(7), 903-909. doi: S0021929002000520

Li, J., Stewart, T. D., Jin, Z., Wilcox, R. K., & Fisher, J. (2013). The influence of size, clearance, cartilage properties, thickness and hemiarthroplasty on the contact mechanics of the hip joint with biphasic layers. *J Biomech, 46*(10), 1641-1647. doi: 10.1016/j.jbiomech.2013.04.009

Li, J., Wang, Q., Jin, Z., Williams, S., Fisher, J., & Wilcox, R. K. (2014). Experimental validation of a new biphasic model of the contact mechanics of the porcine hip. *Proc Inst Mech Eng H, 228*(6), 547-555. doi: 0954411914537618

Machado, M., Moreira, P., Flores, P., & Lankarani, H. M. (2012). Compliant contact force models in multibody dynamics: evolution of the hertz contact theory. *Mechanism and Machine Theory, 53*, 99-121. doi: 10.1016/j.mechmachtheory.2012.02.010

Martin, S., & Sanchez, E. (2013). Anatomy and biomechanics of the elbow joint. *Semin Musculoskelet Radiol, 17*(5), 429-436. doi: 10.1055/s-0033-1361587

Meng, Q., Jin, Z., Wilcox, R., & Fisher, J. (2014). Computational investigation of the time-dependent contact behaviour of the human tibiofemoral joint under body weight. *Proc Inst Mech Eng H, 228*(11), 1193-1207. doi: 10.1177/0954411914559737

Mootanah, R., Imhauser, C. W., Reisse, F., Carpanen, D., Walker, R. W., Koff, M. F., Hillstrom, H. J. (2014). Development and validation of a computational model of the knee joint for the evaluation of surgical treatments for osteoarthritis. *Comput Methods Biomech Biomed Engin, 17*(13), 1502-1517. doi: 10.1080/10255842.2014.899588

Moreira, P., Flores, P., & Silva, M. (2012). A biomechanical multibody foot model for forward dynamic analysis. *2012 Ieee 2nd Portuguese Meeting in Bioengineering (Enbeng)*.

Morrey, B. F. (2000). *The elbow and its disorders*. Philadelphia: N.B. Saunders.

Morrey, B. F., & An, K. N. (1985). Functional anatomy of the ligaments of the elbow. *Clin Orthop Relat Res*(201), 84-90.

Mukras, S., Kim, N. H., Mauntler, N. A., Schmitz, T., & Sawyer, W. G. (2010). Comparison between elastic foundation and contact force models in wear analysis of planar multibody system. *Journal of Tribology, 132*(3), 1-11. doi:10.1115/1.4001786

Perez-Gonzalez, A., Fenollosa-Esteve, C., Sancho-Bru, J. L., Sanchez-Marin, F. T., Vergara, M., & Rodriguez-Cervantes, P. J. (2008). A modified elastic foundation contact model for application in 3D models of the prosthetic knee. *Med Eng Phys, 30*(3), 387-398. doi: S1350-4533(07)00061-6 10.1016/j.medengphy.2007.04.001

Rahman, M., Cil, A., Bogener, J. W., & Stylianou, A. P. (2016). Lateral collateral ligament deficiency of the elbow joint: a modeling approach. *J Orthop Res, 34*(9), 1645-1655. doi:10.1002/jor.23165

Rahman, M., Cil, A., & Stylianou, A. P. (2016). Prediction of elbow joint contact mechanics in the multibody framework. *Med Eng Phys, 38*(3), 257-266. doi: 10.1016/j.medengphy.2015.12.012

Rahman, M., Cil, A., Johnson, M., Lu, Y., Guess, T.M. (2014). Development and validation of a computational multibody model of the elbow joint. *Advances in Biomechanics & Applications, 1*(3), 169-185. doi: 10.12989/aba.2014.1.3.169

Safran, M., Ahmad, C. S., & Elattrache, N. S. (2005). Ulnar collateral ligament of the elbow. *Arthroscopy, 21*(11), 1381-1395. doi: S0749-8063(05)00954-0

Schenck, R. C., Jr., Athanasiou, K. A., Constantinides, G., & Gomez, E. (1994). A biomechanical analysis of articular cartilage of the human elbow and a potential relationship to osteochondritis dissecans. *Clin Orthop Relat Res*(299), 305-312.

Silva, P. C., Silva, M. T., & Martins, J. M. (2010). Evaluation of the contact forces developed in the lower limb/orthosis interface for comfort design. *Multibody System Dynamics, 24*(3), 367-388. doi: 10.1007/s11044-010-9219-6

Spratley, E. M., & Wayne, J. S. (2011). Computational model of the human elbow and forearm: application to complex varus instability. *Ann Biomed Eng, 39*(3), 1084-1091. doi: 10.1007/s10439-010-0224-y

Stormont, T. J., An, K. N., Morrey, B. F., & Chao, E. Y. (1985). Elbow joint contact study: comparison of techniques. *J Biomech, 18*(5), 329-336.

Stylianou, A. P., Guess, T. M., & Cook, J. L. (2012). Development and validation of a multi-body model of the canine stifle joint. *Comput Methods Biomech Biomed Engin*. doi: 10.1080/10255842.2012.684243

Stylianou, A. P., Guess, T. M., & Kia, M. (2013). Multibody muscle driven model of an instrumented prosthetic knee during squat and toe rise motions. *J Biomech Eng, 135*(4), 041008. doi: 10.1115/1.4023982

TekscanWebsite. https://www.tekscan.com/support/faqs/how-does-level-accuracy-change-curvature-surfaces-increases.

Wake, H., Hashizume, H., Nishida, K., Inoue, H., & Nagayama, N. (2004). Biomechanical analysis of the mechanism of elbow fracture-dislocations by compression force. *J Orthop Sci, 9*(1), 44-50. doi: 10.1007/s00776-003-0735-6

Wang, H., Chen, T., Koff, M. F., Hutchinson, I. D., Gilbert, S., Choi, D., Maher, S. A. (2014). Image based weighted center of proximity versus directly measured knee contact location during simulated gait. *J Biomech, 47*(10), 2483-2489. doi: 10.1016/j.jbiomech.2014.04.010

Wang, H., Chen, T., Torzilli, P., Warren, R., & Maher, S. (2014). Dynamic contact stress patterns on the tibial plateaus during simulated gait: a novel application of normalized cross correlation. *J Biomech, 47*(2), 568-574. doi: 10.1016/j.jbiomech.2013.11.042

Wilharm, A., Hurschler, C., Dermitas, T., & Bohnsack, M. (2013). Use of Tekscan K-scan sensors for retropatellar pressure measurement avoiding errors during implantation and the effects of shear forces on the measurement precision. *Biomed Res Int, 2013*, 829171. doi: 10.1155/2013/829171

Willing, R., King, G. J., & Johnson, J. A. (2015). Contact mechanics of reverse engineered distal humeral hemiarthroplasty implants. *J Biomech, 48*(15), 4037-4042. doi: 10.1016/j.jbiomech.2015.09.047

Willing, R., Lapner, M., Lalone, E. A., King, G. J., & Johnson, J. A. (2014). Development of a computational technique to measure cartilage contact area. *J Biomech, 47*(5), 1193-1197. doi: 10.1016/j.jbiomech.2014.01.047

Willing, R. T., Lalone, E. A., Shannon, H., Johnson, J. A., & King, G. J. (2013). Validation of a finite element model of the human elbow for determining cartilage contact mechanics. *J Biomech, 46*(10), 1767-1771. doi: 10.1016/j.jbiomech.2013.04.001

Zhang, X., Blalock, D., & Wang, J. (2015). Classifications and definitions of normal joints. In *Osteoarthritis - progress in basic research and treatment*. ISBN 978-953-51-2136-7. doi: 10.5772/59977

VITA

Mohsen Sharifi Renani was born in Isfahan, Iran. Mohsen attended Emam Mohammad Bagher High School, one of the top three high school in Isfahan. After finishing high school, he started his undergraduate in Mechanical Engineering for one year at Semnan University and then attended to the Isfahan University Technology to continue his study. In the spring of 2014, he graduated with a Bachelor of Science degree in Mechanical Engineering. After graduation, he got admission from University of Missour-Kansas City (UMKC) and moved to United State in fall 2014. He started pursuing his master degree in Mechanical Engineering, with an emphasis on Biomechanics, at UMKC. At the same time, he joined the Musculoskeletal Biomechanics Research Laboratory as a graduate research assistant for more than two years under supervision of Dr. Antonis Stylianou. Mohsen was named the department's Outstanding M.S. student in 2015 and also received Phi Kappa Phi honor from the University in 2016. During his master, Mohsen also attended in Hospital for Special Surgery in the New York, as research engineer intern in summer 2016. He worked closely with research engineers at the Biomechanics department and understood knee functions by performing a series of computational modeling on cadaver knees. At the same year, he began working in the R&D at Zimmer Biomet, a prestigious orthopaedic medical device company, as research engineer for 4 month. There, he obtained a valuable experience and knowledge in orthopaedic medical device industry and could accomplish multiple R&D projects. Over the past two years, Mohsen gained considerable experience at developing a computational model of human joint, design, and evaluating medical devices. Upon completion of his M.S. degree, Mohsen plans to follow his dream as research engineer and entrepreneur in biomechanics by using his education.